CHEMICAL REVIEWS

Review

pubs.acs.org/CR

Ultrahigh-Vacuum Tip-Enhanced Raman Spectroscopy

Eric A. Pozzi,[†] Guillaume Goubert,[†] Naihao Chiang,[‡] Nan Jiang,[§] Craig T. Chapman,[†] Michael O. McAnally,[†] Anne-Isabelle Henry,[†] Tamar Seideman,[†,‡] George C. Schatz,[†] Mark C. Hersam,[†,‡,∥] and Richard P. Van Duyne*[,†,‡]

[†]Department of Chemistry, [∥]Department of Materials Science and Engineering, and [‡]Applied Physics Program, Northwestern University, Evanston, Illinois 60208, United States

[§]Department of Chemistry, University of Illinois at Chicago, Chicago, Illinois 60607, United States

ABSTRACT: Molecule−surface interactions and processes are at the heart of many technologies, including heterogeneous catalysis, organic photovoltaics, and nanoelectronics, yet they are rarely well understood at the molecular level. Given the inhomogeneous nature of surfaces, molecular properties often vary among individual surface sites, information that is lost in ensemble-averaged techniques. In order to access such site-resolved behavior, a technique must possess lateral resolution comparable to the size of surface sites under study, analytical power capable of examining chemical properties, and single-molecule sensitivity. Tip-enhanced Raman spectroscopy (TERS), wherein light is confined and amplified at the apex of a nanoscale plasmonic probe, meets these criteria. In ultrahigh vacuum (UHV), TERS can be performed in pristine environments, allowing for molecular-resolution imaging, low-temperature operation, minimized tip and molecular degradation, and improved stability in the presence of ultrafast irradiation. The aim of this review is to give an overview of TERS experiments performed in UHV environments and to discuss how recent reports will guide future endeavors. The advances made in the field thus far demonstrate the utility of TERS as an approach to interrogate single-molecule properties, reactions, and dynamics with spatial resolution below 1 nm.

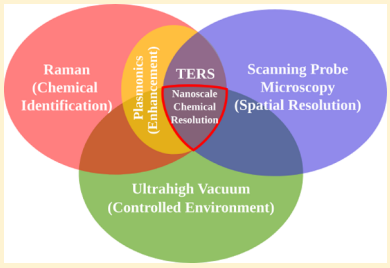

CONTENTS

1. INTRODUCTION

1.1. Motivation

Numerous technological fields have undergone extensive miniaturization in recent decades, edging deeper and deeper into the nanoscale. Embodying this trend, the packing density of transistors on integrated circuits has doubled every 2 years since Gordon Moore predicted such a phenomenon in 1975.[1] Marking the ultimate goal in miniaturization, the field of molecular electronics seeks to realize fundamental units of logic constructed from individual molecular building blocks.[2] As technology shrinks, from millimeter to micrometer to nanometer length scales, so must the resolution of analytical techniques capable of characterizing such systems. Even in fields not explicitly dedicated to miniaturization, nanoscale

Special Issue: Vibrational Nanoscopy

Received: June 1, 2016
Published: December 22, 2016

DOI: 10.1021/acs.chemrev.6b00343
Chem. Rev. 2017, 117, 4961−4982

chemical and physical interactions are critical to performance in real, inhomogeneous media. As an illustrative example, efficiency in heterogeneous catalysis is greatly impacted by atomic-scale features.[3]

An ideal characterization tool possesses the capability to understand fundamental nanoscale interactions. Sensitivity down to the single-molecule (SM) limit enables the detection of localized phenomena. The most powerful tools will be able to not only visualize individual molecules but also probe their structure and interactions with their environments. Such capabilities are possible using tip-enhanced Raman spectroscopy (TERS), particularly when operated in ultrahigh-vacuum (UHV) environments. We begin by introducing analytical approaches capable of nanoscale resolution, chemical characterization, and single-molecule sensitivity, highlighting spectroscopic techniques.

1.2. Nanoscale Spectroscopy

There are important incentives to probe molecular structure and properties at the nanoscale. With such resolution, one can interrogate localized physical phenomena with applications ranging from understanding material properties that are enhanced by engineered nanostructures[4−6] to studying and explaining augmented chemical reactivity at undercoordinated atoms or at metal/oxide interfaces on a catalyst.[7−9] As a result, significant effort has been geared toward developing techniques with nanoscale spatial resolution. Transmission electron microscopy (TEM) and scanning probe microscopy (SPM) are examples of well-established techniques capable of accessing detail with atomic resolution.

SPM techniques in particular are attractive because they are versatile, operating in many experimental conditions (pressure, temperature), and they do not involve high-energy electrons that can damage molecular adsorbates. The two most prominent techniques in the SPM family are scanning tunneling microscopy (STM) and atomic force microscopy (AFM). Both of these microscopies have been applied to studies of interfaces at the nanoscale in many fields of science.[10−13] Both STM and noncontact-mode AFM (NC-AFM), a method using a mechanical resonator to transform the force experienced by the probe into a frequency shift, have been used to achieve atomic resolution of surface-bound molecules and inorganic solids.[14,15] STM is the primary SPM modality used in UHV-TERS and will hence be our focus in this review.

In STM, a sharp metallic tip is brought very close to a conducting or semiconducting sample and a bias voltage is applied between the tip and the sample to allow the tunneling current to flow from one to the other (Figure 1). The tunneling current (I_t) is extremely sensitive to the distance between the sample and the tip, with a change of distance between the tip and the sample (the gap) of 0.1 nm, increasing the current by roughly an order of magnitude.[16] For a very simple model of the tip and in the limit of weak coupling between the tip and the sample, it can be shown that the tunneling current is proportional to the local density of states (LDOS) at the Fermi level of the sample at the position of the tip.[16] As a result, the tunneling current contains a mixture of topological and electronic information. In the most common mode of operation, the tunneling current is maintained constant in a feedback loop by changing the gap distance with a piezoelectric actuator. Another pair of piezoelectric actuators is used to scan the tip in the plane of the sample, while the apparent height of the sample under constant-current feedback is recorded to produce an image. In typical imaging conditions for adsorbed molecular species, the STM tip is expected to be at a distance > 3 Å from the sample to avoid contact and degradation of the STM resolution.[17]

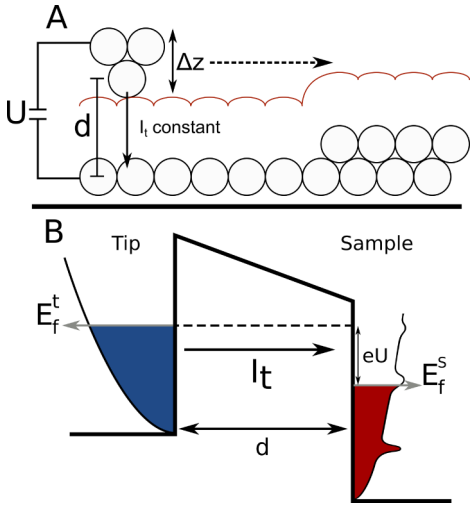

Figure 1. (A) Principle of the STM showing the tip at a distance d from the sample. U is the amplitude of the bias in Volts. I_t is the tunneling current, which can flow from the tip to the substrate or from the substrate to the tip (the former is depicted here). The tip moves perpendicular to the sample to maintain constant current. (B) STM principle in terms of energy levels; bias induces current flow from the tip into energy levels of the sample.

In optical spectroscopy, diffraction imparts a fundamental resolution limit to techniques in which reflective or refractive optics are used to focus light. As a result, visible light cannot be confined to length scales beyond ∼200 nm. Effort has been dedicated to surpassing the optical diffraction limit in order to increase spatial resolution in optical spectroscopy. Super-resolution microscopy provides a means to circumvent this limitation by fitting the point spread function of a diffraction-limited spot to a two-dimensional Gaussian.[18−20] Given a nonlinear intensity response or a spatial modulation of the signal in time, centroids of the fits of successive acquisitions can be used to build up an optical image of the sample. Fluorescence signals are commonly imaged using super-resolution techniques with resolution on the order of tens of nanometers.[21,22]

1.3. Chemical Characterization

As evidenced above, advances in STM have provided detailed information about the topography and physical properties of surface systems at the nanoscale.[23] However, STM had been lacking chemical specificity until the development of STM-inelastic electron tunneling spectroscopy (IETS). STM-IETS has made it possible to measure the vibrational spectrum of a molecule adsorbed on a solid surface by detecting tunneling paths facilitated by energy transfer from tunneling electrons to molecular vibrations.[24,25] The major setback of this technique, however, is that samples must be measured with exceptional mechanical stability and at cryogenic temperatures to avoid thermal smearing of electron energies. In addition, the vibrational modes detected using STM-IETS have poorly understood selection rules,[25] and therefore, the information gained is limited compared to other vibrational spectroscopies. The signal/noise ratio is usually very low in STM-IETS, but recent progress was made using tip-enhanced IETS, which

DOI: 10.1021/acs.chemrev.6b00343
Chem. Rev. 2017, 117, 4961−4982

allowed the analysis of individual hydrogen bonds at a water−salt interface.[26]

The most common optical spectroscopic techniques capable of high chemical information content have utilized excitation ranging in energy from X-rays to the infrared (IR) within the electromagnetic spectrum of light. Extended X-ray absorption fine structure (EXAFS), X-ray excitation spectroscopy (XES, sensitive to occupied electronic states),[27] and X-ray Raman spectroscopy (XRS) measure the oxidation states of individual elements directly through core−shell excitations of electrons.[28,29] Each technique is bulk sensitive but can be extended to surface and interfacial characterization with grazing incidence geometries.[30] However, a synchrotron source is usually required to obtain high-quality spectra.

In contrast, optical vibrational spectroscopies (IR and Raman spectroscopy) are much more experimentally accessible and also provide chemically specific information about molecules and structures. The two techniques offer similar vibrational information but exploit different physical processes. In IR spectroscopy, incident light is directly absorbed by the sample when the excitation energy matches that of a molecular vibration, thereby promoting the molecule to a vibrationally excited state. In Raman spectroscopy, an excitation photon induces a dipole in a molecule, which then reradiates a photon in a scattering process. During this process, the induced dipole can transfer energy to a vibrational mode (Stokes scattering) or vice versa (anti-Stokes scattering) in the amount equal to one vibrational quantum. The intensity ratio between the anti-Stokes and the Stokes Raman lines relates to the population of the vibrationally excited states and thus can be used as a temperature probe.[31,32] Both Raman and IR spectroscopies offer complete and complementary "vibrational fingerprints" of molecular analytes, but sensitivity is typically weaker in the case of Raman spectroscopy. However, the inelastic scattering nature of the Raman process allows excitation wavelengths to be adjusted to overlap with system resonances,[33] enabling dramatic increases in sensitivity.

1.4. Single-Molecule Sensitivity

Up until the late 1980s it was thought that detecting individual molecules using light was impossible. The disparity between the wavelength of light and the size of a molecule renders their interaction weak. As such, spectroscopy relied on ensemble detection of molecules to obtain detectable signals. While this approach may be suitable for homogeneous media or for when knowledge of the average structure is sufficient, it cannot reveal nanoscale inhomogeneities that generally exist in real systems. In addition, it requires large quantities of material, which is not always possible. As a result, great effort was directed toward increasing spectroscopic sensitivity to the SM level.

Moerner and Kador reported the first optical detection of an individual dye molecule in 1989 using absorption spectroscopy.[34] Immobilization of molecules in a solid matrix combined with liquid helium cooling narrowed the molecular absorption feature and increased the optical cross section to a detectable level. One year later, Orrit and Bernard demonstrated SM fluorescence detection on the same molecular system.[35] Given the drastically higher signal/noise ratio of the fluorescent signal, fluorescence became the standard for SM detection moving forward.

An obvious limitation of fluorescence lies in the fact that only systems with strong radiative decays can be detected. The technique has been generalized to other molecules through their covalent modification to introduce fluorescent labels. However, such modification often perturbs the natural behavior of the labeled molecule as a result of the physical size or photochemical activity of the fluorescent label.[36] In addition, photobleaching and blinking of the fluorophore limit the robustness of the technique.[37] Thus, detection of absorption and scattering signatures is an appealing alternative.

Plasmonic enhancement of external optical fields using noble metal nanostructures provides a means of increasing the strength of light−matter interactions to levels compatible with SM sensitivity. One method of achieving SM detection is through probing the optical resonance of the plasmonic structure. Since plasmon energy, and hence particle scattering wavelength, is sensitive to minute changes in the local refractive index, several groups have demonstrated detection of SM binding events using this approach.[38−41] However, this technique comes with implicit downsides. First, refractive index sensing is not chemically specific. Second, indirectly detecting the presence of a molecule restricts knowledge about its actual location.

All of the techniques mentioned above detect individual spectral features and thus give poorer structural information content than, for example, vibrational spectroscopy, which allows the structure of analytes to be discerned through analysis of their vibrational fingerprints. For this reason, there is large interest across the scientific community in the fields of TERS and surface-enhanced Raman spectroscopy (SERS), which use plasmon resonances to efficiently couple far-field irradiation to length scales comparable to the size of single molecules, thus increasing their effective optical cross sections. As will be discussed further below, these approaches have allowed for routine detection of individual molecules while simultaneously enabling the characterization of their structures and, in the case of TERS, their locations at the nanoscale.

1.5. Scope of the Review

In this review we cover reported experimental work in the field of tip-enhanced Raman spectroscopy performed in vacuum environments. We specifically highlight UHV-TERS experiments, in which complete in situ sample preparation and analysis can be performed under pressures in the low 10^{-10} Torr range and below, resulting in the greatest elimination of contaminants and small molecules (e.g., water) and the highest quality imaging; however, this review will also cover reports of TERS performed in a high-vacuum (HV) environment. To orient the reader and to provide an accurate account of the field, selected TERS experiments performed in ambient are covered as they relate to the topics discussed. For a thorough coverage of the field of TERS as a whole we point the reader to a number of recent reviews on the subject.[42−51] In the next section, we will discuss SERS, a predecessor of TERS, which is also well reviewed elsewhere.[51−55]

2. PLASMONICS AND SERS

2.1. Background

Anomalously high Raman scattering intensity from molecules adsorbed to a roughened Ag electrode was first observed in 1974[56] and described as a surface phenomenon 3 years later.[57,58] The field of SERS, comprising thousands of research articles in the years since, was born. Much attention was paid to the physics underlying the signal amplification in the following decade or so,[59] but up until the late 1990s the majority of

DOI: 10.1021/acs.chemrev.6b00343
Chem. Rev. 2017, 117, 4961−4982

researchers were using SERS as a complementary analytical tool in the fields of electrochemistry, surface catalysis, and so on.

The field of SERS encountered a resurgence in 1997, when two groups reported evidence of SM detection using SERS.[60,61] This capability attracted broad interest, as it enabled vibrational spectroscopy to be performed in the absence of ensemble averaging. Initial SMSERS reports relied on arguments based on intensity fluctuations and quantized intensity distributions to statistically claim SM detection. A more robust verification method, termed the bianalyte approach, followed.[62−65] Here, two spectroscopically distinct molecules were probed simultaneously, and detection of individual analytes suggested SM detection. However, difficulties arising from differing Raman cross sections and adsorption behavior complicate analysis in bianalyte experiments.[66,67]

Dieringer et al. refined this concept to verify SM detection using isotopically labeled molecules, which possess equivalent physical properties but exhibit unique vibrational signatures.[68] Analysis of individual spectral events using combined Poissonian−binomial statistics comprises a strong argument for SM detection. The isotopologue approach has since been utilized to verify SM sensitivity with different isotopically labeled molecular pairs,[69] including naturally occurring ones,[70] and on lithographically fabricated substrates.[71,72]

2.2. Enhancement Mechanisms

After the discovery of SERS, two proposed theoretical mechanisms were widely discussed: the chemical (CHEM) and electromagnetic (EM) mechanisms. Both the CHEM and the EM mechanisms were heavily researched from theoretical and experimental perspectives.[59,73−75] Briefly, the EM mechanism can be thought of as a coupled-dipole system, in which the molecular and plasmonic dipoles can feel the response induced by optical excitation in one another. In nanostructured metals having dielectric functions with large negative real and small positive imaginary components, a plasmon is excited by incident irradiation. Collective oscillations of conductance electrons produce a locally intense EM field that enhances optical processes in other dipoles in the near field. If a molecule is in the near field of the plasmon, it will feel both the incident unperturbed irradiation as well as the enhanced plasmonic field. Incoherently scattered light can again be coupled to the plasmon, such that both the incident and the emitted fields are enhanced. Arising from the $|E|^2$ enhancement of both the excitation and the scattering processes, the widely discussed $|E|^4$ enhancement of SERS comes from treatment of the SERS scattering process by the EM mechanism.[76] Enhancement of optical fields in the near field of coupled dipoles is commonly referred to as the local field effect (LFE). The LFE has been fully developed to understand numerous experimental observations in SERS.[77−79] Experimentally, the EM mechanism has consistently shown enhancement magnitudes on the order of 10^6−10^8 over normal Raman scattering.[76,80]

Chemical contributions to signal enhancement have also been considered. Early experimental work by Campion et al. isolated the effects of the CHEM mechanism, wherein the authors observed a low-energy absorbance feature for pyromellitic dianhydride (PMDA) on Cu(111) that was not observed for the individual components.[81] This feature was assigned to a charge-transfer (CT) state that contributed to enhancement of the resulting SER signal. However, the Raman response was only enhanced by a factor of 30 as a result of the CT resonance, much less than the 10^6−10^8 supplied by the EM mechanism. Electronic resonances, whether they arise from the static electronic structure or from a new charge-transfer resonance due to changes in the electronic structure due to chemical interaction of the analyte with the local surface, will be wavelength dependent. However, the vast majority of experimental and theoretical studies have consistently shown enhancement on the order of 10^2, with the highest theoretical prediction of 500 from Moore et al.[82] Morton et al. reported additional theoretical work on the CHEM mechanism, describing in detail the specific cases involved in charge-transfer resonances.[83,84] Morton and Jensen discovered that both metal-to-ligand and ligand-to-metal CT resonances occur in molecule−substrate systems, contributing enhancement magnitudes up to 10^2. As the field of SERS has progressed, reports have repeatedly shown that the CHEM mechanism acts at very short distances with a maximum enhancement of 1 or 2 orders of magnitude.[76,83]

2.3. Improving SERS Spatial Resolution

The optical diffraction limit prevents SERS signals from being spatially resolved beyond ∼200 nm using conventional microscopy. Multiple groups have sought to increase spatial resolution in SERS by applying super-resolution microscopy techniques to SER signals emanating from plasmonic hot spots.[85−89] Diffusion of molecules within hot spots provides intrinsic signal modulation for the application of super-resolution microscopy, enabling imaging of SER signals from plasmonic hot spots with an order-of-magnitude improvement in resolution over the optical diffraction limit (Figure 2).[19] Recently, randomly modulating the phase of the incident beam was observed to fill in the gaps in the image between hot spots.[90]

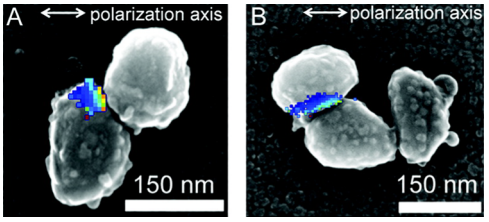

Figure 2. SERS spatial intensity map and corresponding SEM image for a (A) single-junction and (B) two-junction nanostructure. Spatial intensity maps are qualitatively overlaid on the SEM images based on the geometry of the nanoparticles. Polarization of the excitation light is shown. Reprinted with permission from ref 19. Copyright 2012 American Chemical Society.

Additional strategies have been employed to overcome the diffraction limit in SERS. One such approach involves physically confining an optical beam within the aperture at the end of a metal-coated fiber, a technique named scattering near-field optical microscopy (SNOM).[91] The aperture probe is scanned across a surface and allows for <50 nm resolution. The Zenobi group imaged nanostructured Ag surfaces using SNOM, reporting resolution down to 70 nm.[92,93] Deckert and co-workers then applied the technique to detect catalytic intermediates on a Pt-coated SERS substrate.[94] It is important to note that SNOM can operate in the absence of surface enhancement; however, sensitivity in this case is insufficient to detect the Raman response of individual molecules.

Applying super-resolution microscopy and SNOM to SERS substrates in principle enables one to resolve SER signals below

DOI: 10.1021/acs.chemrev.6b00343
Chem. Rev. 2017, 117, 4961−4982

the optical diffraction limit, but their utility in mapping molecular species is still limited by the spatial inhomogeneity of electromagnetic field strength on fabricated SERS substrates. In other words, the origins of the SER signal in these techniques are in fixed locations defined not by the distribution of analyte but rather by the distribution of surface enhancement, and increased resolution merely allows researchers to locate electromagnetic hot spots. In order to circumvent this restriction and directly image molecular species using plasmonics, it is necessary for an imaging modality to offer control over the location of the enhancing region. Ideally, one would like the capability to move a hot spot across a surface and detect signals from arbitrarily chosen locations. This is the concept behind TERS.

3. TERS

3.1. Background

Over 30 years ago, John Wessel first proposed a methodology for augmenting optical fields at the nanoscale.[95] The reported concept involved performing STM with a plasmonic particle as the scanning probe. The particle enhances and localizes the electromagnetic field of an incident beam within a small volume at the particle−surface junction, while incorporation of STM enables precise control of the particle location. This technique, which would become known as TERS, combines the sensitivity of Raman spectroscopy, the lateral resolution of SPM, and the sensitivity of SERS (Figure 3).

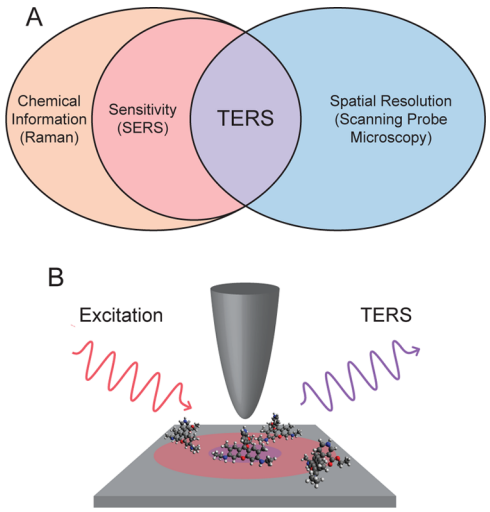

Figure 3. (A) Venn diagram highlighting the benefits of TERS. (B) Basic schematic of the TERS experimental geometry. A plasmonic tip augments the excitation and scattered fields within a confined volume at the tip−sample junction, supplying spatially resolved and detailed structural information on surface-bound species down to the SM level.

This proposed approach was experimentally demonstrated 15 years later, when multiple groups used metal or metal-coated tips to augment the Raman signal of surface-bound molecules.[96−99] These first TERS reports were performed on inverted optical microscopes, in which an objective focused laser excitation and collected scattered light from below the surface, which was required to be transparent. In the coming years, TERS optical methodologies utilizing refractive side-illumination[100−103] and top-illumination[104] optics as well as parabolic mirrors[105,106] were developed, allowing researchers to study opaque samples, including the single-crystalline materials often studied in UHV. Since TERS is a specific case of SERS, the selection rules are usually thought to be the same. Alternative selection rules have been proposed for HV-TERS[107] involving the observation of IR bands in the TER spectrum, but no rationale for the existence of selection rules specific to HV-TERS compared to ambient or UHV-TERS has been presented. In the UHV-TERS studies presented in this review, special selection rules were not needed for the analysis of spectra; DFT- or TDDFT-based calculations offered a satisfactory explanation.[108−111]

Significant effort has been dedicated to exploiting the lateral control offered by scanning probe techniques in order to chemically map systems at the nanoscale. Tip-enhanced Raman imaging involves collecting a TER spectrum at each pixel of a corresponding scanning probe image. A TER image can then be constructed by mapping an optical signal (e.g., the integrated intensity of a particular TERS peak) over the scanned area. The Novotny group reported an early example of TER imaging (Figure 4), wherein the authors demonstrated simultaneous

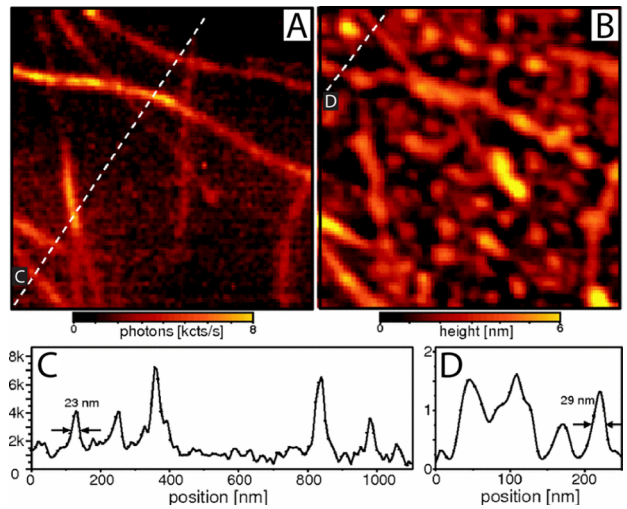

Figure 4. Simultaneous TER image (A) and AFM image (B) of SWCNTs on glass. Scan area 1 × 1 μm. Raman image is acquired by detecting the intensity of the G' band upon laser excitation at 633 nm. No Raman scattering signal is detected from humidity-related circular features present in the topographic image. (C) Cross section taken along the indicated dashed line in the TER image. (D) Cross section taken along the indicated dashed line in the AFM image. Height of individual tubes is ∼1.4 nm. Vertical units are photon counts per second for C and nanometers for D. Reprinted with permission from ref 112. Copyright 2003 by The American Physical Society.

AFM and TER imaging of single-walled carbon nanotubes (SWCNTs).[112] The TER image was constructed by plotting the intensity of the SWCNT G' band at each pixel. TER imaging lateral resolution of ∼25 nm was reported, a number that has since been improved by over an order of magnitude. Lateral resolution in TERS will be discussed in detail in section 4.2.

SM sensitivity in TERS was a major goal since the first TER spectra were reported. Although localizing the probe beyond the optical diffraction limit reduces inhomogeneity in the collected signal compared to conventional Raman microscopy, TERS is not truly site specific unless signals from individual molecules can be detected. The first claims of SM sensitivity were based on arguments regarding molecular coverage and

DOI: 10.1021/acs.chemrev.6b00343
Chem. Rev. 2017, 117, 4961−4982

signal intensity fluctuations and distributions.[113,114] One claim of SM sensitivity was derived from the correlation of single-molecule junction formation and breakage with TER signal intensity in a technique called fishing-mode TERS.[115] The first direct verification of SM detection in TERS was reported in 2008, when Steidtner and Pettinger collected a TER image of a single brilliant cresyl blue (BCB) molecule on Au(111).[116] Subsequently, Sonntag et al. statistically verified SM detection using the previously discussed isotopologue approach.[117]

3.2. Tip Enhancement

3.2.1. Mechanisms. The mechanisms responsible for the increased enhancements seen in TERS experiments are largely the same as those involved in SERS, namely, the EM and CHEM mechanisms. As is the case for SERS, the EM mechanism is the dominant contributor and will be our focus here. In addition to studies highlighted here, which represent the leading school of thought in the TERS community since its early years, several groups have made progress in elucidating the quantum mechanical nature of TERS enhancements that may lead to high lateral resolution, as will be discussed in section 4.2.2.

In TERS a sharp, plasmonically active, conducting tip serves to generate the enhancement field involved in EM, in contrast to the metal surface in SERS. The geometry of the tip allows for a markedly increased concentration of excess surface charges at its apex, leading to intense, highly spatially localized electromagnetic fields. Approaching the tip within close (~1−2 nm) proximity to a plasmonic substrate further increases field intensity and confinement. Here the tip and surface plasmons couple to produce a spatially confined field in the space between the tip and the substrate, a phenomenon known as the gap-mode effect. The enhancement in the narrow active region of this coupled tip−substrate system has been shown to follow a d^{-10} dependence, where d is the distance between the tip and the substrate.[118]

Many other factors are involved in determining the nature of the confined field, including tip material and geometry as well as incident laser polarization, wavelength, focus, and relative angle.[42] Several recent theoretical studies have used finite-difference time-domain (FDTD) modeling and analytical theory to explore EM for various tip−substrate geometries and material combinations in the search for an optimal apparatus.[119−124] In all cases, the tip has been represented as an idealized smooth structure. In FDTD simulations a structure that approximates the last 100 nm or so at the bottom of the tip is employed. This strategy leads to many discrete resonator-like plasmon multipoles[119] rather than the more continuous plasmon excitation profile that is seen for infinite structures employed in analytical models.[124] However, at wavelengths in the UV region an LSPR originating from the spherical tip apex can be observed in all cases. Most recently, Yang et al.[122] and Kazemi-Zanjani et al.[125] used FDTD to elucidate the localized enhancement of tips in the presence and absence of metallic surfaces. Both studies show field enhancements concentrated at the apex of the tip when the surface is dielectric, while spatial confinement of the gap plasmon becomes evident in the presence of a metallic surface. Kazemi-Zanjani et al. also investigated polarization-dependent properties of the spatially confined plasmon and found that depending on the polarization of the incident irradiation one can selectively create field nodes or large enhancements at the tip apex (Figure 5).[125]

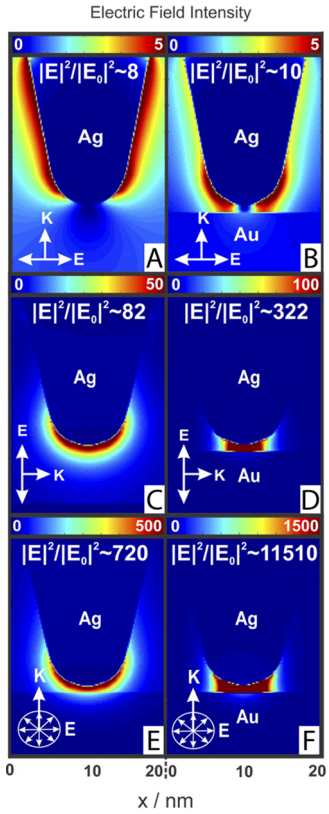

Figure 5. Electric field distribution at the 10 nm apex of a silver tip illuminated at 532 nm by (A) linearly polarized light propogating along the tip axis, (B) linearly polarized light propagating along the tip axis with 1 nm separation between tip apex and gold substrate, (C) light linearly polarized along the tip axis propagating perpendicular to the tip axis, (D) light linearly polarized along the tip axis propagating perpendicular to the tip axis with 1 nm separation between tip apex and silver substrate, (E) radially polarized light propagating along the tip axis, and (F) radially polarized light propagating along the tip axis with 1 nm separation between tip apex and gold substrate. Adapted with permission from ref 125. Copyright 2013 Optical Society of America.

Highlighting the importance of materials selection on the EM in TERS, Meng et al. used FDTD, in addition to experiments, to show that EM enhancements of up to 10^5 can be achieved using a bare AFM tip and can be attributed to the lightning rod effect.[126] They also present what they consider to be the optimal configuration for Au-coated AFM tip−substrate system. Here they optimized the tip, incident field, and substrate to find that a 5 nm layer of Au on a Si AFM tip achieved the best enhancement that balanced tip sharpness, and hence resolution, with enhancement.

It should also be noted that proper TERS electrodynamics models should include both the incident and the outgoing fields. Schatz and Ausman showed that dipole reradiation can lead to far-field spatial inhomogeneities in the signal at the detector.[127] These factors become more pronounced when the incident radiation and the detector are nonorthogonal. This highlights the need to account for dipole emission effects rather than just determining the standard $|E(\omega)|$ enhancement factor.

3.2.2. Enhancement Factor. Quantification of tip enhancement is useful in order to understand the local electromagnetic field intensity that a sample experiences and to compare experimental configurations and apparatuses. This

DOI: 10.1021/acs.chemrev.6b00343
Chem. Rev. 2017, 117, 4961−4982

is typically done through calculating the enhancement factor (EF) using the equation

$$\mathrm{EF} = \frac{I_{\mathrm{nf}}/N_{\mathrm{nf}}}{I_{\mathrm{ff}}/N_{\mathrm{ff}}}$$

where I_{nf} and I_{ff} are the near-field and far-field intensities and N_{nf} and N_{ff} are the corresponding numbers of molecules contributing to each signal.[128] Equivalently, near-field and far-field areas can be used in place of N_{nf} and N_{ff}.

I_{nf} cannot be directly measured, since a TERS measurement contains the far-field signal originating from all molecules within the laser focus. As a result, I_{nf} is typically calculated by subtracting the signal with the tip retracted from the surface from that with the tip engaged. In other words, $I_{\mathrm{nf}} = I_{\mathrm{TERS}} - I_{\mathrm{ff}}$. In many cases the far-field signal is not strong enough to be detected. In this case the magnitude of the noise serves as an upper bound for the far-field intensity, and hence, the calculation gives a lower bound for the EF. Far-field signal intensity can also be evaluated by measuring on the same apparatus the Raman response of probe molecules in a larger ensemble, such as in solution, from which a larger signal emanates.

N_{ff} can be calculated using the surface coverage of analyte and the area of the laser focus. In the case that I_{ff} is determined from a solution measurement, N_{ff} can be calculated using the concentration of the solution and the focal volume of the beam waist. N_{nf} is more difficult to evaluate (except in the case of SMTERS, in which $N_{\mathrm{nf}} = 1$) because the area of the enhancing region is not always known. A method to approximate the area of the near field was presented in 2005, when Pettinger et al. calculated the radius of the enhanced field to be one-half the radius of curvature of the tip.[129] The most accurate method of determining the near-field area is through TER imaging. Here, a line profile of the TER signal over a one- or zero-dimensional feature gives the lateral response of tip enhancement, whose width can then be characterized.[130]

EFs exceeding 10^7 can be achieved in TERS experiments,[113,114,131] providing sufficient sensitivity for SM detection if a suitable analyte is studied with laser excitation resonant with a molecular electronic transition. Since plasmonic enhancement is proportional to $|E|^4$,[132] these values correspond to an amplification of the electric field magnitude in the tip−sample junction by ∼100×. It is important to note that these values are not inclusive of resonance enhancement, which further increases sensitivity but is not related to the mechanisms of tip enhancement. Another commonly reported metric for tip enhancement is contrast, which is calculated as $I_{\mathrm{TERS}}/I_{\mathrm{ff}}$. However, EF is a more accurate quantification of tip enhancement than contrast, since contrast is not directly related to the magnitude of optical field enhancement and is influenced by the size of the laser focus in a given apparatus.

3.3. Resonance Enhancement

Normal Raman spectroscopy is typically considered a low-sensitivity technique, having optical cross sections on the order of 10^{-29}−10^{-26} cm^2 molecule^{-1}.[133] While enhancements of 10^6−10^8 are common in TERS, tip enhancement alone is generally insufficient for SM detection, which requires optical cross sections near 10^{-16} cm^2 molecule^{-1}.[60,61] However, if the excitation energy overlaps with one of the electronic transitions of the molecule of interest, the molecule is excited into a real electronic/vibronic excited state, which can provide an additional ∼10^5-fold increase in signal intensity (i.e., resonance enhancement).[133] Thus, the combination of tip and resonance enhancements enables SM sensitivity. Although one needs to be mindful of photochemistry associated with the electronic excitation of molecules, the excitation power in TERS is generally below 1 mW and would not trigger intense photochemical reactions, at least for CW excitation. The use of UHV conditions also prevents all reaction mechanisms relying on external oxidation agents, such as water or oxygen. This technique is more rigorously termed tip-enhanced resonant Raman spectroscopy (TERRS); however, we will use the term TERS when describing reports performed under resonance Raman scattering conditions in agreement with previous literature.

Besides increasing sensitivity in TERS, resonant excitation also provides information about the nature of excited electronic/vibronic states. The nature of a molecular transition can be visualized using a Raman excitation profile of the absolute and relative mode intensities in a wavelength-scanned experiment.[134,135] One can also distinguish electronic and vibronic transitions of a molecule using a Raman excitation profile.[110] Figure 6 depicts a simulated tip-enhanced resonance

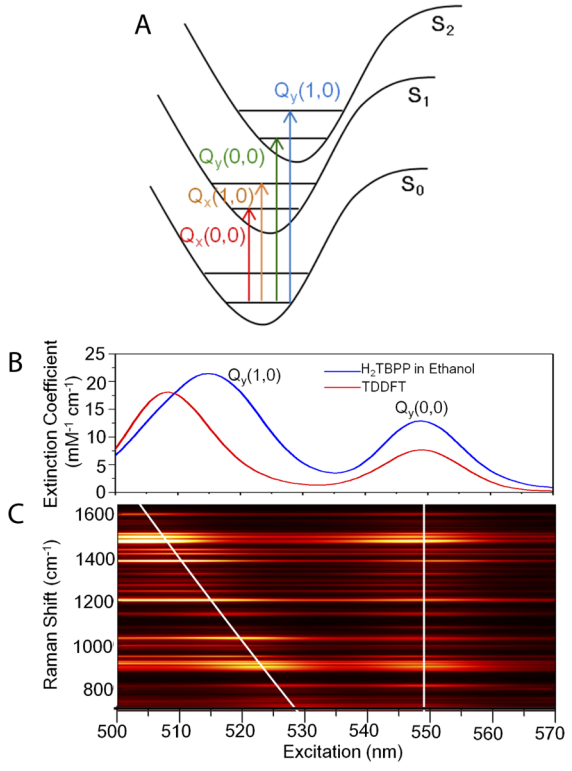

Figure 6. (A) Schematic of the optical transitions in a metal-free porphyrin (H_2TBPP). (B) Experimental and time-dependent density functional theory (TD-DFT)-simulated extinction of H_2TBPP. (C) TD-DFT-simulated resonance Raman excitation profile of H_2TBPP. White lines indicate the corresponding $Q_y(1,0)$ and $Q_y(0,0)$ excitation energies for each vibrational modes. Adapted with permission from ref 110. Copyright 2015 American Chemical Society.

Raman excitation profile of a porphyrin molecule by time-dependent density functional theory (TD-DFT). In the top-down waterfall plot (Figure 6C), the maximum intensity of each normal mode with excitation overlapping the $Q_y(0,0)$ transition exists near the center of the absorption band, representative of an electronic transition. In contrast, $Q_y(1,0)$ is a vibronic transition, and therefore, the position of the

DOI: 10.1021/acs.chemrev.6b00343
Chem. Rev. 2017, 117, 4961−4982

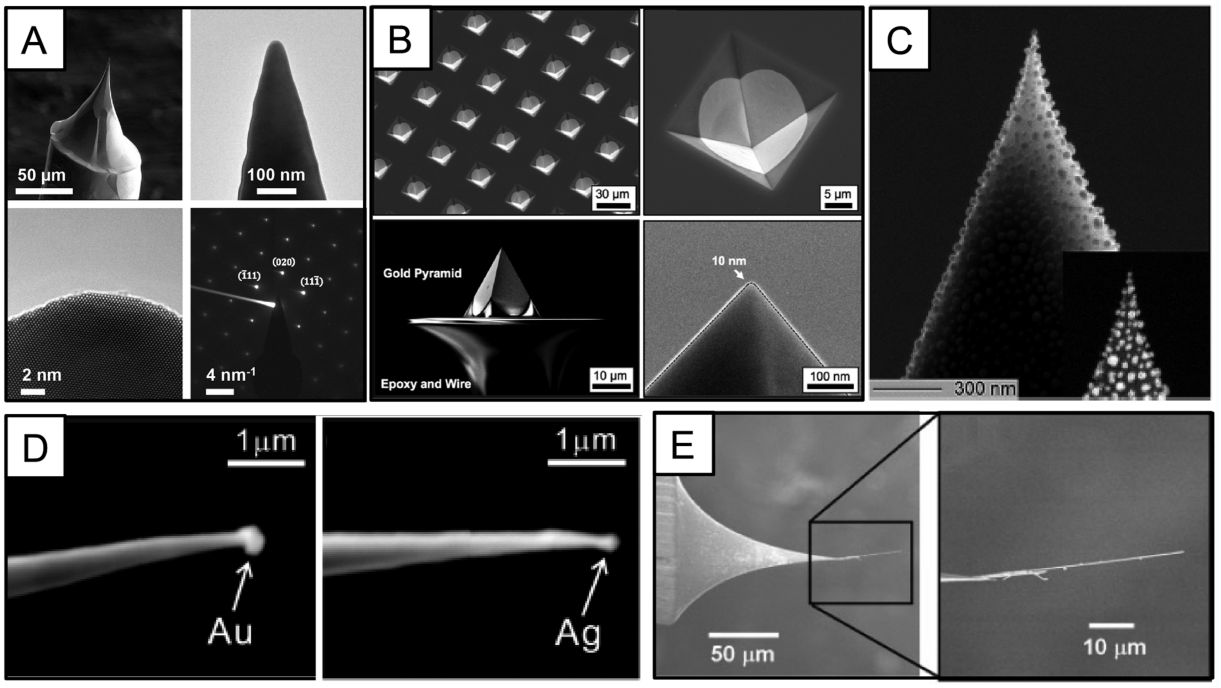

Figure 7. Sampling of tip fabrication methods using top-down (A–C) and bottom-up (D, E) approaches. (A) Au tip fabricated by electrochemical etching and characterized by SEM (top left), TEM (top right and bottom left), and electron diffraction (bottom right).[139] (B) Massively parallel microfabrication of Au tips characterized by SEM.[140] (C) Ag deposition on a silicon AFM cantilever with a single nanoparticle at its apex, as evidenced by SEM.[141] (D) SEM images of a W tip covered with a Au nanosphere (left) or a Ag nanosphere (right).[142] (E) SEM images of a W tip with Ag NWs under different magnifications.[143] Adapted with permission from refs 139, 140, 141, 142, and 143. Copyright 2015 American Chemical Society, 2012 American Chemical Society, 2015 Royal Society of Chemistry, 2006 American Chemical Society, and 2010 John Wiley & Sons, Ltd., respectively.

maximum intensity of different normal modes depends strongly on whether the excitation is close to the first vibronic excited state of each mode.

3.4. Tip Fabrication

The fabrication of tips suitable for TERS relies on several parameters related to the technical requirements of the scanning probe methodology used and the fabrication constraints of engineering materials with nanoscale precision.[136] The most important requirement for a tip to be TERS active comes from the plasmonic material, typically Ag or Au, from which it is made. In the ultraviolet, Al is also a viable option, as experimentally demonstrated by Kawata and coworkers[137] and simulated by Yang et al.[138] While Ag tips provide the strongest plasmonic response, they are highly reactive with oxygen or sulfur species present in ambient conditions. Therefore, limiting atmospheric exposure of a freshly fabricated Ag tip through immediate use or through transfer to an inert environment (e.g., UHV) is ideal for optimizing lifetime. The reproducibility of tip fabrication and the variability of enhancement among tips limit consistency within TERS apparatuses and across research groups. Here we address approaches for fabricating efficient and robust tips while considering reproducibility and throughput.

Fabrication of tips with nanoscale plasmonic features can be done by both top-down and bottom-up approaches (Figure 7). First, we examine top-down approaches. Electrochemical etching allows for high-throughput tip fabrication and is easily the method most used for the construction of STM-TERS tips. Starting with a Ag or Au wire with a diameter of a few hundred micrometers, etching can produce a conical tip with a radius of curvature at the apex of a few tens of nanometers. To electrochemically etch tips, the Ag[144,145] or Au[146] metal wire serves as the anode and is immersed (~2–3 mm) in an electrolyte solution and placed in the center of a circular cathode. Incorporating potentiostatic control[147,148] or optical feedback from a witness camera[149] during the etching process can be implemented to prevent overetching. Modifications to the etching process, including the application of dc pulses to the tip, allow further tip shape and texture control.[150] In AFM-TERS, the most commonly used fabrication method is another high-throughput, top-down technique, in which metal is deposited on commercially available AFM cantilevers through thermal evaporation or physical vapor deposition.[96,141,151] In postprocessing, groups have demonstrated that the far-field signal in TERS can be minimized by irradiating a focused-ion-beam-milled grating[152,153] or single groove[139] on the STM or AFM tip shaft instead of irradiating the tip–sample junction. Here, the grating launches surface plasmons to the tip apex, preventing far-field irradiation molecules outside of the enhancing region; however, this benefit comes at the expense of throughput. An electrochemical deposition method for the fabrication of AFM-TERS tips has been demonstrated for Au deposition in aqueous solution with control of the tip apex radius.[154]

Tip-to-tip variability is a major limitation in tips constructed using electrochemical etching or metal deposition, leading some researchers to pursue alternative fabrication methods in an effort to improve reproducibility while maintaining throughput. Johnson et al. reported parallelized fabrication of Au pyramids by anisotropically etching pyramidal wells in a silicon wafer using KOH and depositing Au.[140] After lift off of the etching mask, Au pyramids can be template stripped using a

DOI: 10.1021/acs.chemrev.6b00343
Chem. Rev. 2017, 117, 4961–4982

droplet of epoxy and a tungsten wire to yield a functioning, conductive TERS tip. A variant of this method utilizing angled metal deposition into the etched wells produces asymmetric metal pyramids with tunable plasmon frequencies.[155]

Efforts have also been devoted to fabricating TERS tips with bottom-up approaches involving grafting plasmonic (Au or Ag) nanoparticle(s) onto existing tips. Groups have demonstrated fabrication of plasmonic probes by mounting Au nanoparticles onto nonplasmonic tips.[142,156,157] You et al. reported using alternating current dielectrophoresis for grafting individual Ag nanowires to W wires with demonstrated TERS activity.[143] In addition, Kim et al. demonstrated in situ growth of a Ag-coated Au nanoparticle at the apex of an AFM tip.[158] Finally, electrochemical deposition of plasmonic nanoparticles at the conductive apex of a nanoprobe enables reproducible tips whose optical properties can be tailored.[159,160] Such methods allow researchers to tailor physical properties of constructed tips, such as plasmon frequency, for particular applications.

3.5. Environmental Control

The achievement of a highly controlled environment can be approached in a liquid medium, which hinders the diffusion of airborne contaminants. When using high-purity solvents with a residual content of impurities at or below 1 ppb, it is possible to prevent fouling of surfaces and electrodes for the duration of a typical experiment.[161] In proof-of-concept experiments, the Zenobi group demonstrated TERS in a liquid environment and observed decreased formation of carbonaceous photodecomposition products.[162,163] More recently, TERS has been performed in electrochemical cells using both AFM[151] and STM[164] apparatuses. In these studies, TERS was used to study the surface of an electrode under potential control and measure the response of adsorbed molecules to the electrode potential. Zeng et al. monitored the potential-dependent protonation of (4′-(pyridin-4-yl)biphenyl-4-yl)methanethiol (4-PBT) on Au(111).[164] Increased signal stability in this experiment was attributed to either better heat dissipation or decreased O_2 in water compared to in air. The Van Duyne group observed the first charge-transfer reaction using TERS.[151] Reversible reduction of Nile blue molecules on an indium tin oxide surface was observed to correspond with a loss of TER signal due to the loss of the resonance condition. TERS voltammograms were constructed using the TER intensity recorded during forward and reverse potential sweeps.

Limitations of TERS in liquid exist, however. The number of well-defined surfaces that can be probed in a liquid environment is limited. Studies must be performed on relatively inert substrates, such as graphite and gold, which are not degraded under ambient conditions on the time scale of the experiment. It must be noted that even for these surfaces, as long as they are prepared ex situ, a layer of adsorbed organic airborne contaminants will be present as contact angle measurements have shown.[165,166] Importantly, molecule−solvent interactions influence the behavior of the system and must be disentangled from the molecule−surface interactions one also wishes to study. Nevertheless, these studies demonstrate the benefits of performing TERS in well-controlled environments. Many different molecules and materials can be deposited in UHV, as shown by the extensive UHV STM/AFM literature, although complex biological samples are difficult to reproduce in UHV conditions. Although UHV-TERS cannot match the electrochemical capabilities possible in liquid TERS apparatuses, we will describe in the next section how UHV environments uniquely allow for pristine conditions for TERS experimentation.

4. UHV-TERS

4.1. History and Benefits

Given the sensitivity of TERS and SPM, environmental control is at a premium in order to avoid spurious signals in TER spectra or features in topographic images. Open-air environments provide many opportunities for contamination of the sample surface. In addition to airborne contaminants, AFM measurements have confirmed the existence of a water meniscus several nanometers thick on surfaces at moderate humidity.[167,168] In addition to introducing contaminants through diffusion, this meniscus can alter the surface interactions that researchers desire to probe with TERS.

Pristine surface conditions are attainable when studies are performed in UHV. UHV environments additionally prevent degradation of the tip. As we will describe in this section, performing TERS in UHV also increases the stability of molecules within intense electromagnetic fields and provides the capability of low-temperature operation. While UHV operation provides many benefits, spectroscopy becomes more difficult when a UHV chamber is involved. By using ex situ laser focusing and Raman collection optics, optimization of the optical path can be achieved straightforwardly and without compromising vacuum. On the other hand, in situ optics allow for closer placement of focusing optics and thus tighter focusing and a larger solid angle of collection.

In 2007, the Pettinger group reported the design and operation of a custom-built UHV-TERS apparatus.[105] The authors mounted an optical platform with all necessary optical elements to a rigid frame containing the STM. In 2008, they demonstrated the first correlated UHV-TERS and STM mapping of a single BCB molecule, reporting a lateral resolution of 15 nm.[116] The UHV environment was also shown to decrease the rate of molecular photobleaching, enabling longer data collection times. In 2009, the Maultzsch group reported their development of an AFM-based TERS apparatus in UHV along with UHV-TER spectra of rose bengal.[169] Both groups prepared their samples using solution deposition prior to introduction into UHV, which may compromise surface cleanliness and imaging quality.

When sample preparation and molecular deposition are performed entirely in vacuo, atomically clean surfaces can be maintained with only the molecule(s) of interest present. This greatly enhances the stability of the tip−sample junction and ensures minimal contamination in the field enhancement region beneath the STM tip. Utilizing these advantages, the Van Duyne group demonstrated detection of multiple vibrational modes in UHV-TERS of copper phthalocyanine (CuPc) on Ag(111) concurrent with molecular-resolution STM imaging (Figure 8A).[148] Subnanometer STM resolution revealed the 2D packing arrangement of the CuPc adlayer as well as boundaries between individual ordered domains. In 2014, the Wolf group reported a TERS study of graphene nanoribbons prepared on a Au(111) surface under UHV conditions (Figure 8B).[170] Molecular-resolution imaging provided topographical characterization during the polymerization process and corroborates the signal detected in UHV-TERS. In 2013, Zhang et al. demonstrated <1 nm resolution on an isolated porphyrin, resolving in the process the macrocycle of the nonmetalated molecule.[108]

DOI: 10.1021/acs.chemrev.6b00343
Chem. Rev. 2017, 117, 4961−4982

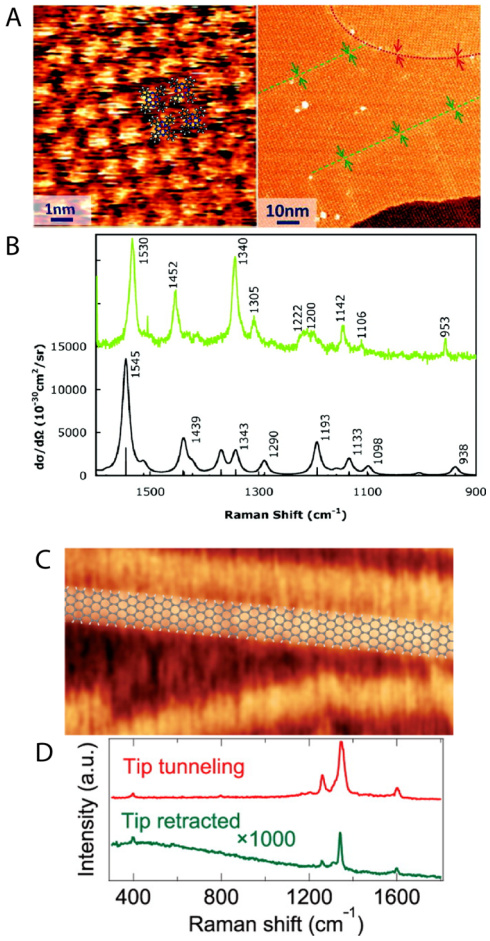

Figure 8. (A) Molecular-resolution topographic STM images of a copper phthalocyanine (CuPc) adlayer on Ag(111) with the tip illuminated by the 633 nm continuous-wave laser, and (B) corresponding UHV-TERS (green) plotted with a TD-DFT-simulated spectrum (black).[148] (C) Molecular-resolution topographic STM imaging and (D) UHV-TERS of graphene nanoribbons (GNRs) fabricated on Au(111) by the on-surface polymerization technique under UHV conditions.[170] Adapted with permission from refs 148 and 170. Copyright 2012 American Chemical Society and 2014 American Chemical Society, respectively.

4.2. Lateral Resolution

4.2.1. Demonstrations <5 nm. A major advantage afforded by TERS in comparison to other optical spectroscopies is its capability of resolving signals with sub-5 nm precision. In contrast to SNOM, spatial resolution in TERS is not limited by the size of the aperture; indeed, resolution beyond the physical size of the tip used has been demonstrated. In 2008, the Pettinger group demonstrated ∼15 nm lateral resolution in TERS of an individual BCB molecule.[116] Lateral resolution was consistent with their previously proposed model,[129] in which the radius of the enhancing region was ∼1/2 the radius of curvature of the probe used. However, recent work, including results by both the Kawata and the Deckert groups, have demonstrated lateral resolution below 2 nm in ambient TERS.[141,171,172]

In UHV, correlated STM and TER imaging have been applied to distinct surface-bound molecular systems: an isolated, immobile molecule[108] or nanostructure;[173] two distinct, adjacent analyte domains;[109] and a single analyte forming different phases on a surface[111] or adopting two discrete conformations.[174] Dong and co-workers first demonstrated subnanometer lateral resolution on an isolated porphyrin molecule under liquid nitrogen cooling.[108] The obtained TER images allow for visualization of the inner structure of a single molecule (Figure 9A). Also demonstrated

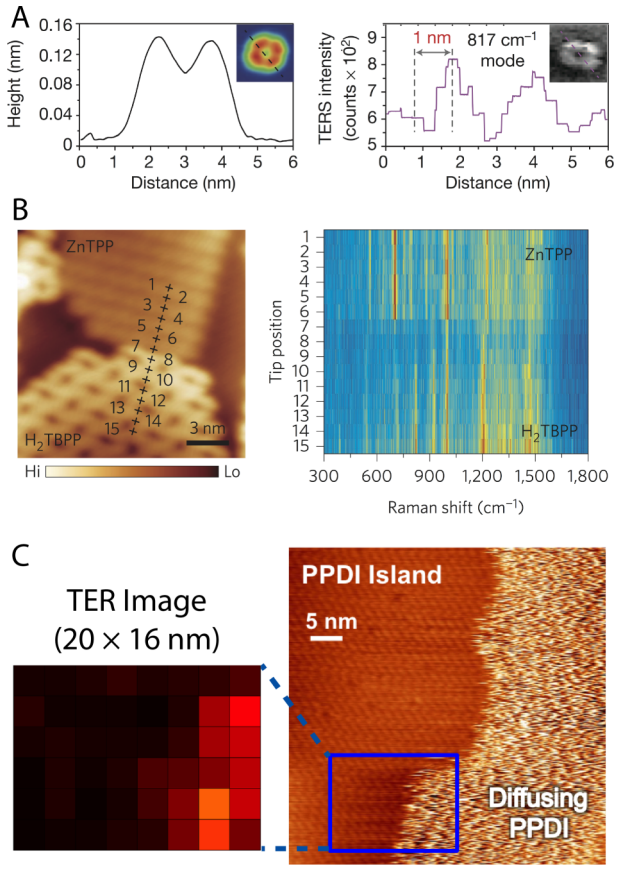

Figure 9. (A) Subnm resolution TER image of an isolated porphyrin molecule at 80 K. Reprinted by permission from Macmillan Publishers Ltd.: *Nature*, copyright 2013.[108] (B) Approximately 0.5 nm resolution TERS mapping of adjacent porphyrin molecules at 80 K. Reprinted by permission from Macmillan Publishers Ltd.: *Nat. Nanotechnol.*, copyright 2015.[109] (C) TER imaging of a dynamic 2D phase boundary of a perylene diimide derivative (PPDI) at room temperature. Reprinted with permission from ref 111. Copyright 2016 American Chemical Society.

in this work was the ability to correlate the observed Raman signal with the local environment of a molecule through TER imaging of a molecule overlapping a surface step edge. The same group also demonstrated 0.7 nm resolution on a carbon nanotube at low temperature in UHV, revealing that TERS can map the spatial extent of local defects as well as the strain resulting from nanotube bending.[173] Utilizing the high resolution of TER imaging under UHV conditions, Jiang et al. unambiguously distinguished two distinct porphyrin molecules aggregated into separate molecular island domains on a silver substrate at 80 K,[109] ∼0.5 nm lateral resolution allowed the spectral signatures of adjacent, but structurally different, molecules to be distinguished (Figure 9B). Chiang et al. recently demonstrated lateral resolution of 0.26 nm on a porphyrin monolayer on Cu(111).[174] This resolution allowed the authors to differentiate between neighboring molecules adopting separate conformations, buckled up or buckled down

DOI: 10.1021/acs.chemrev.6b00343
Chem. Rev. 2017, 117, 4961−4982

from the substrate, and demonstrated that TERS can be used to probe adsorbate−metal interactions.

Also performed under UHV conditions, a dynamic two-dimensional (2D) phase boundary has been imaged by TERS under room-temperature conditions.[111] In this study, the condensed phase (molecular island) and the 2D gas phase of a perylene diimide derivative coexist on the Ag surface. Collected TER images exhibit ∼4 nm lateral resolution using a line scan over the dynamic phase boundary (Figure 9C). Here, the measured resolution is a convolution of the intrinsic TERS resolution and the dynamic width of the phase boundary. Also demonstrated in this study, TERS exhibits increased intensity in the 2D gas phase relative to the condensed phase as a result of different molecular dipole orientation. Therefore, TERS provides access to molecular adsorption geometries even in regions where little STM topographical information is available. Since Raman scattering is sensitive to the orientation of molecules and their molecular structures, TERS is sensitive to the orientation of the molecule relative to the polarization of the local field. In resonance Raman, the orientation of the transition dipole will also affect which modes can be observed, as demonstrated in the report by Jiang et al.[111] In the usual TERS geometry, in which the incoming polarization is parallel to the tip axis, molecular modes that lie in the plane of the surface are less likely to be observed than those with an appreciable perpendicular component. This gives significant power to TERS for site-specific surface analysis, since different adsorption sites can be resolved for the same chemical structure.

UHV-TERS has set the stage for future molecular resolution chemical imaging studies. Clearly, the original explanation for lateral resolution derived purely from classical electrodynamics is insufficient to explain resolution below 5 nm. A detailed discussion of recent attempts with more advanced theoretical approaches is presented in the following section.

4.2.2. Theoretical Explanations. Explaining the exceptional lateral resolution UHV-TERS, in particular the subnanometer resolution from Zhang et al.[108] and Jiang et al.,[109] has been of great interest to the theoretical community in recent years. This area of research is young, stemming from the first demonstration of TERS lateral resolution at the subnanometer limit in 2013.[108] As a result, explanations for the source of these observables are still ongoing. Here we provide an analysis of the recent theoretical work in this area.

Roelli et al. explored theoretically the effects of the optomechanical cavity on surface-enhanced Raman scattering and observed nonlinear plasmonic enhancement in certain physical limits.[175] The theory of the optomechanical cavity applied to SERS and TERS relies on a coherent coupling between the molecular vibrations (mechanical oscillator) and the localized surface plasmon (electromagnetic cavity). The molecular vibration perturbs the plasmon such that the instantaneous plasmon occupancy changes which then acts back on the molecular vibration. The optomechanical cavity behavior is shown schematically in Figure 10A along with a generalized molecule−plasmon system (Figure 10B). If incident laser intensity approaches a parametric instability threshold, at which the rate of backaction amplification exceeds that of intrinsic damping, a strong nonlinear Raman response is observed (Figure 10C). The nonlinear Raman response can be interpreted as a possible explanation to the high lateral resolution demonstrated in TERS. However, we note that the ∼2 × 10^6 W/cm^2 power density giving rise to this effect

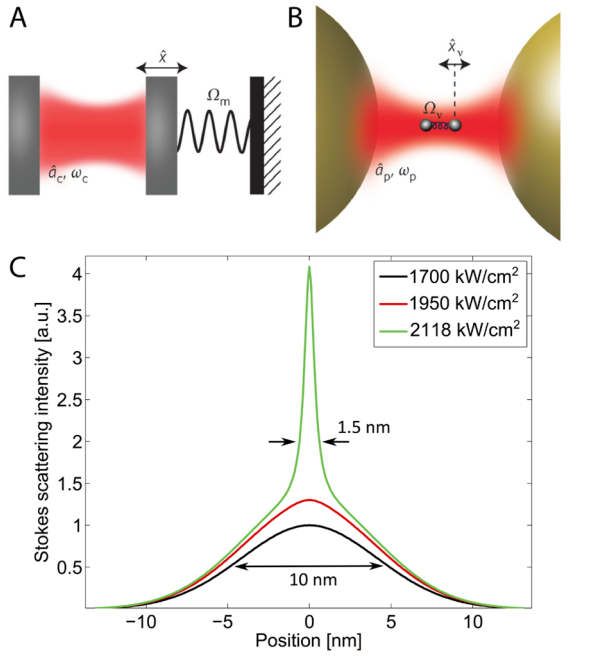

Figure 10. Increased lateral resolution explained by the molecular cavity optomechanics model.[175] (A) System demonstrating the coupling of a mechanical oscillation Ω_m with a cavity of frequency ω_c with occupation $\hat{a}_c$. As the oscillation Ω_m acts on the system, it changes the physical confinement of the cavity in $\hat{x}$. (B) Adapting the system in A to a coupled molecule-plasmon system. (C) Comparison of theoretical Stokes scattering intensity as a function of lateral position from a point-source scatterer at the origin and a Gaussian plasmonic field of 10 nm fwhm. At high field strengths, a strong nonlinear response is observed leading to an increased spatial resolution. Reprinted by permission from Macmillan Publishers Ltd.: *Nat. Nanotechnol.*, copyright 2016.[175]

exceeds power densities used in <5 nm TERS reports, which are in the range 10^2−10^5 W/cm^2.[108,109,111,171,172] For example, the subnanometer resolution experiments of Zhang et al. and Jiang et al. employed power densities of 10^2 W/cm^2.[108,109]

Other nonlinear Raman scattering justifications for exceptional TERS lateral resolution have suggested that TERS can be effectively described by stimulated Raman scattering (SRS).[176−178] These reports develop a theory of SRS where the two fields, a Raman pump and a Raman probe, are provided by the incident laser and the optical plasmon response to the incident laser. Using the higher order confinement from SRS, Duan et al. calculated higher lateral resolution in TERS by the nonlinear Raman effects compared to normal SERS effects (Figure 11).[176] However, there is a discontinuity between TERS experiments and the SRS theory developed. In particular, the experiments done were on molecular electronic resonance, which gives rise to dispersive lineshapes in equivalent resonant femtosecond stimulated Raman scattering (FSRS) experiments due to the interference of multiple Feynman pathways for the light−matter interaction.[179]

Finally, we discuss two theoretical approaches previously applied to SERS that have been implemented to gain understanding about TERS resolution: the image field effect[180] and electric field gradient effects.[178] The image field effect of SERS, originally proposed by Schatz and co-workers,[181] was considered by the Li group as a self-interaction of the molecular dipole with an image dipole in the substrate.[180] The stronger spatial dependence of self-interaction leads to higher lateral

DOI: 10.1021/acs.chemrev.6b00343
Chem. Rev. 2017, 117, 4961−4982

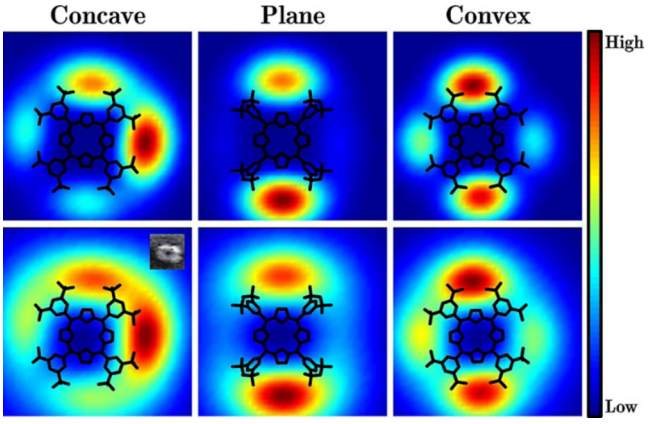

Figure 11. Comparison of nonlinear (top) and total (bottom) tip-enhanced Raman images of a H_2TBPP molecule under concave, planar, and convex configurations by a plasmonic field with a fwhm of 20 Å.[176] Inset in the bottom left image is the experimental data from ref 108. As seen, the nonlinear Raman response can lead to tighter confinement for the Raman image and higher lateral resolution. Reprinted with permission from ref 176. Copyright 2015 American Chemical Society.

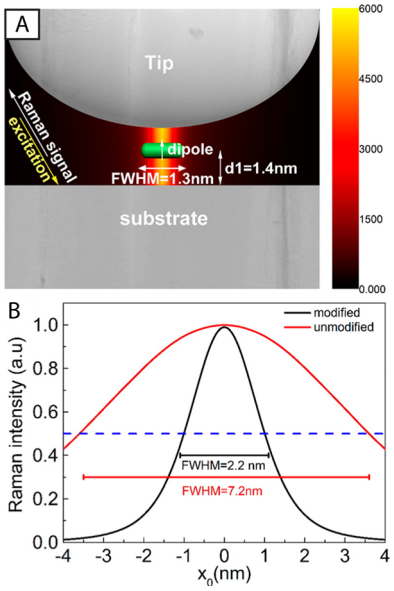

Figure 12. Image field effect in TERS.[180] (A) Diagram of coupled molecular dipole−nanogap TERS system. (B) Comparison of TERS lateral resolution in the cases of no molecular self-interaction (red) and inclusion of molecular self-interaction (black). Including for the self-interaction leads to higher lateral resolution in TERS. Reprinted with permission from ref 180. Copyright 2015 American Chemical Society.

resolution in TERS as shown in Figure 12. The rationale of the higher lateral resolution comes from the self-interaction relying on multiple elastic scattering events within the Ag tip−substrate gap. While this theory does provide a higher lateral resolution than that predicted by conventional EM mechanisms, it does not reach the subnanometer resolution observed. In addition, work from Marinica et al. suggests the spatial regime where image field and self-interaction effects would strongly contribute is overtaken by quantum plasmonic effects.[182] The effect of electric field gradients on lateral resolution in TERS was explored by Meng et al., who considered a system of H_2TBPP molecules interacting with a plasmonic tip.[178] The authors show that electric field gradients can lead to higher TERS lateral resolution than predicted by traditional EM mechanisms; however, these effects occur in very small tip−substrate distances where, again, quantum plasmonic effects are expected to contribute greatly.[182,183]

Explanations for the source of high lateral resolution TERS imaging in the subnanometer limit are still ongoing. Mechanisms relying on optomechanical cavities suggest experimental power regimes that are experimentally inaccessible. SRS mechanisms lead to unobserved experimental signatures. Finally, other mechanisms, including image dipole effects,[180] electric field gradients,[178] and nonresonant chemical effects,[184] rely on distance regimes that have stronger quantum plasmonic effects. Such effects have been predicted to result in a quantum upper limit for field confinement[185] as well as in shifts in plasmon resonances but have yet to be observed in TERS. Hence, more theoretical studies on high-resolution TERS are necessary to fully understand the mechanism(s) responsible for the experimentally observed resolution.

4.3. Low-Temperature Operation

Cryogenic UHV-TERS is a promising approach for unraveling the intricacies of adsorbate−substrate interactions that are inaccessible by other means. UHV-TER spectra of rhodamine 6G (R6G) on Ag(111) under liquid helium cooling (19 K) narrowed in comparison with room-temperature TER spectra, resulting from decreased inhomogeneous broadening (Figure 13A).[186] Peaks were also observed to shift at low temperature, revealing additional chemical information about the adsorbate−substrate interactions. Specifically, the orientation of R6G on Ag(111) was determined and corroborated by time-dependent density-functional theory (TD-DFT) calculations. This report indicates that the spectral character in UHV-TERS can be used to determine molecule−surface interactions.

Low-temperature operation also enables the characterization of properties that cannot be examined at room temperature. For example, molecular diffusion is slowed or prevented, spectral features are narrowed, and probe stability is increased upon cooling. Exceptional probe stability enabled Zhang et al. to obtain the highest TERS resolution reported to date, as described above.[108] Raschke and co-workers reported a temperature-dependent study of malachite green (MG) on template-stripped Au using a shear-force AFM operated under high-vacuum conditions.[187] Between 90 and 300 K, six TER spectra were acquired at varying temperatures. As expected, the Raman peaks narrowed with decreasing temperature (Figure 13B), and several of them split, revealing new peaks that the authors attributed to intramolecular coupling. These signal characters allowed the authors to characterize molecular properties and dynamics including vibrational dephasing, intramolecular coupling, and molecular rotation. Future studies will be aimed toward interrogating surface interactions at individual adsorption sites, which will allow researchers to discern structural, physical, and chemical properties of individual molecules and nanostructures in specific environments without the effects of ensemble averaging.

4.4. Probing Chemistry

The high chemical content and sensitivity of SERS make it a valuable probe to follow the advancement of reactions under varied experimental conditions.[188−190] It appears natural then to use the higher spatial resolution of TERS to follow reactions at the nanoscale. As an additional benefit, the versatility of

DOI: 10.1021/acs.chemrev.6b00343
Chem. Rev. 2017, 117, 4961−4982

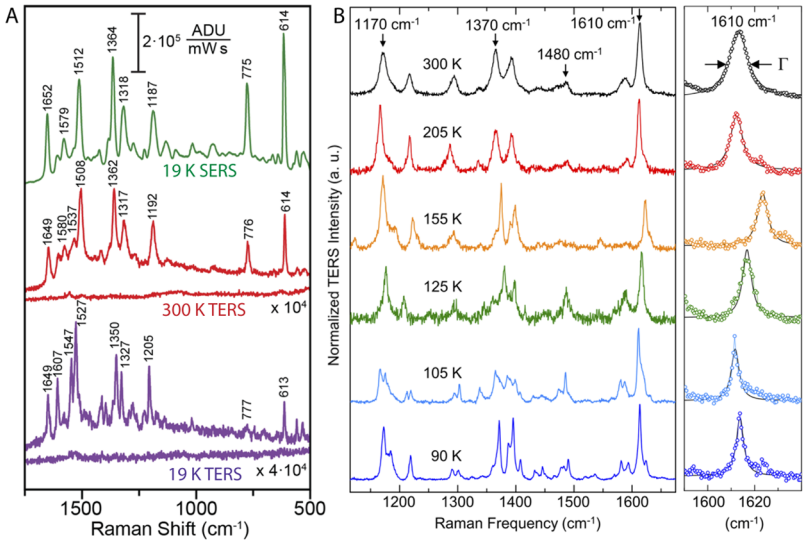

Figure 13. (A) UHV-TERS peaks at 19 K are narrowed and shifted compared to UHV-SERS at 19 K and UHV-TERS at 300 K. Surface diffusion of rhodamine 6G (R6G) is suppressed at 19 K. R6G adsorption geometry on Ag(111) can be characterized by the differences between the 300 and the 19 K UHV-TERS. Adapted with permission from ref 186. Copyright 2014 American Chemical Society. (B) Peak narrowing in temperature-dependent TERS. Spectra are background subtracted and intensity normalized. Lorentzian line fit analysis of the N−C stretch mode at 1610 cm^{-1} as an example (right graph of A, narrowest spectra are selected from a large data set). Reprinted with permission from ref 187. Copyright 2015 American Chemical Society.

TERS allows its use on a variety of materials,[151,191] enabling experiments on catalytically relevant surfaces beyond Ag and Au. Ideally, probing single-site catalytic efficiency will be possible.

Highly concentrated electromagnetic energy in the tip−sample junction can be used to trigger localized reactions using the incoming light or the resulting plasmon. One of the model reactions is the dimerization of *p*-nitrothiophenol (pNTP) or *p*-aminothiophenol (pATP) to *p*,*p*′-dimercaptoazobisbenzene (DMAB) on Au or Ag.[193] This dimerization reaction has been studied by TERS using an AFM operated in ambient conditions.[192] A dual-wavelength setup was used, with 532 nm irradiation triggering the reaction and 633 nm excitation probing the TERS response in order to monitor the reaction. Results were analogous to previous SERS studies, with DMAB peaks emerging after 532 nm irradiation (Figure 14). More recently, the dimerization of pATP on Ag was imaged using TERS, in which 20 nm resolution was demonstrated.[194] HV-TERS reports described similar findings using an STM tip to induce dimerization.[195] Perhaps stemming from ex situ sample preparation, the lack of molecular resolution prevented the imaging of local surface structure and molecular coverage.

Tallarida et al. studied the photoinduced isomerization of an individual molecule at the apex of an STM-TERS tip in UHV.[196] The authors characterized assemblies of flat [4-(phenylazo)phenoxy]hexane-1-thiol (ABT) molecules on Au(111) but were not able to visualize TERS or induce photoisomerization of molecules within the 2D layer. However, they measured TERS from an outlier molecule, from which signal persisted when the tip was retracted from the surface; it was thus attributed to a molecule adsorbed on the tip. Two characteristic spectra were observed and assigned to the cis and trans isomers of ABT, and single-molecule sensitivity was inferred from the bimodal and anticorrelated nature of these signals in the collected TER spectra (Figure 15). The ability to measure single-molecule TERS on the tip was attributed to an unexpected resonant enhancement due to a different electronic absorption compared to the solid form and to a better alignment of the transition dipole with the field polarization compared to flat-lying molecules on the surface. Since the molecule was on the tip, this is not a typical TERS experiment as it does not provide spatially resolved information about species on a surface. Nonetheless, it provides insight into chemical processes at the single-molecule level.

Although several steps were achieved on the way to the monitoring of single molecules with TERS in well-controlled conditions, the full potential of UHV-TERS has not yet been achieved. While ambient studies have shown 20 nm resolution for the dimerization of pATP, recent development in high-resolution UHV-TERS suggest that it should be possible to achieve <1 nm resolution in monitoring chemical events of individual molecules.

To consider what can be done, it is useful to examine studies performed with STM[197,198] or NC-AFM[199,200] at cryogenic temperatures. In these cases, single-molecule reactions can be triggered by tunneling electrons and studied down to individual chemical bonds. Unstable intermediates have been characterized,[200] indicating a path to study many reaction mechanisms from the single-molecule standpoint. This particular approach is limited to cryogenic temperatures, which are attainable in UHV-TERS systems. While STM imaging of individual bonds is limited to planar molecules, TERS allows for structural characterization of species having more complex geometries. The addition of vibrational spectroscopy to the arsenal of single-molecule reaction characterization tools will substantially increase the number of chemical systems that can be studied.

4.5. Toward Ultrafast TERS

Processes occurring at ultrafast time scales are critical to the function of chemical systems. Vibrational motion, proton transfer, and transition state formation and destruction, to name a few, take place on time scales of 1 ns or faster.[201] In order to spectroscopically investigate such transient processes and species, nonlinear optical techniques are required. Ultrafast

DOI: 10.1021/acs.chemrev.6b00343
Chem. Rev. 2017, 117, 4961−4982

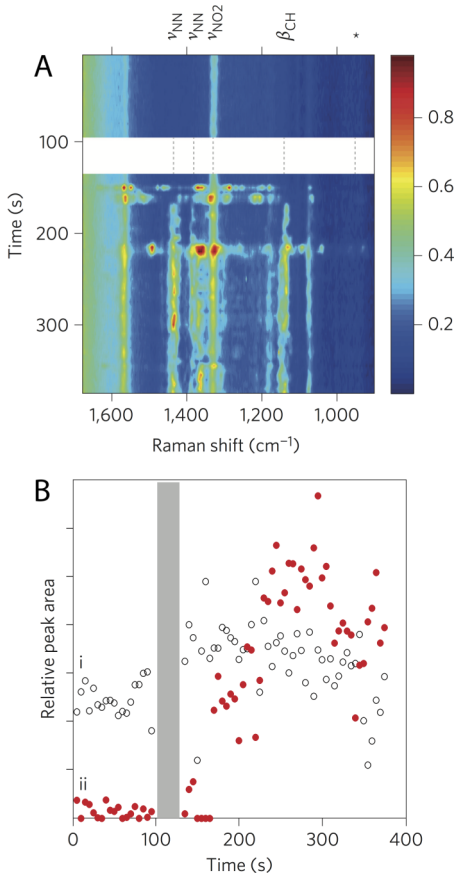

Figure 14. (A) Time-dependent TERS spectra at 633 nm excitation (5 s integration time, 380 μW) shown before (top) and after (below white band) 532 nm illumination.[192] (B) Peak areas as a function of time for the pNTP band at 1335 cm^{-1} and for the band at 1440 cm^{-1}, belonging to DMAB. The period of green illumination between 100 and 130 s is indicated by the shaded band. Reprinted by permission from Macmillan Publishers Ltd.: *Nat. Nanotechnol.*, copyright 2012.[192]

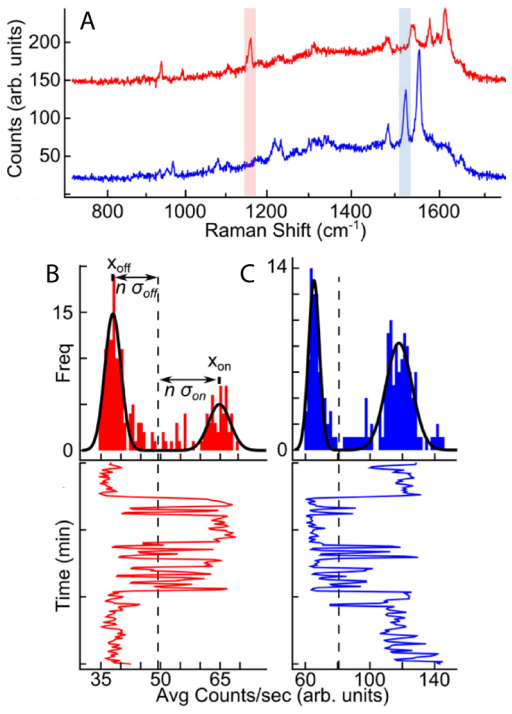

Figure 15. Single-molecule isomerization revealed by UHV-TERS:[196] (A) two characteristic spectra observed during the experiment; (B) 1160 cm^{-1} and (C) 1524 cm^{-1} bands integrated in a 9 cm^{-1} window showing binomial distribution (top) and anticorrelated behavior (bottom). Adapted with permission from ref 196. Copyright 2015 American Chemical Society.

Raman techniques typically involve pulses compressed to one picosecond or shorter and enable such transient processes to be observed. While the temporal resolution of traditional pump–probe Raman techniques is limited owing to the time–bandwidth product of ultrashort laser pulses, coherent Raman spectroscopies, such as FSRS and coherent anti-Stokes Raman scattering (CARS), allow kinetics on time scales of tens of femtoseconds to be discerned.[202] Extending these studies to the nanoscale may become possible upon incorporating ultrafast spectroscopic techniques with TERS. A great challenge in doing so lies in the perturbation of the probed system by the high local EM fields experienced at the tip–sample junction under irradiation by ultrashort pulses. These pulses are produced in a pulse train operated at a fixed frequency (commonly from 100 kHz to 100 MHz). As a result, duty cycles, which refer to the fraction of time the system is active, in ultrafast spectroscopy are on the order 10^{-9}–10^{-4}. Peak powers within ultrashort pulses are then orders of magnitude higher than the average power of the laser. However, in an effort to keep the signal above the noise in ultrafast spectroscopy, modest average laser power must be used, resulting in transiently intense fields within each individual pulse.

It is well known that energy flow within ultrashort pulses can be strong enough to damage irradiated media.[203] In fact, this characteristic has led to the use of laser pulses for material removal with micrometer or better precision in areas including micromachining and ophthalmic surgery. When combined with plasmonic enhancement, near-field intensity can become prohibitively high with respect to molecular and nanostructure damage. As discussed above, the electric field is enhanced on the order of 100× in a TERS junction. The effects of plasmonic enhancement and pulsed excitation then compound, resulting in instantaneously intense near-field strengths. Multiple groups have demonstrated the morphological changes, including complete melting, that can occur when plasmonic structures are irradiated by ultrafast pulses.[203,204] Even more sensitive to ultrashort pulses are the organic analytes typically studied in plasmonically enhanced ultrafast experiments, which can readily undergo physical and chemical modifications in these environments.[205] In a previous report of plasmonically enhanced ultrafast Raman spectroscopy, namely, surface-enhanced femtosecond stimulated Raman spectroscopy (SE-FSRS), a clear plateau in signal gain was observed with increasing power of the Raman pump (1 ps pulses), which the authors attribute to a damage mechanism involving either the probed molecules or the plasmonic substrates.[206]

The Van Duyne group previously conducted experiments to assess the feasibility of integrating pulsed laser excitation with TERS. Klingsporn et al. collected TERS of R6G and malachite green isothiocyanate (MGITC) in ambient conditions using 1 ps pulses from an optical parametric oscillator (OPO) with a repetition rate of 80 MHz.[207] Spontaneous TERS was successfully collected, but the signal was observed to decay irreversibly on the time scale of tens of seconds. If the tip was moved to a different surface location within the laser focus, however, the signal would transiently reappear. Signal decay was thus attributed to a molecular damage mechanism as

DOI: 10.1021/acs.chemrev.6b00343
Chem. Rev. 2017, 117, 4961–4982

opposed to one involving damage to the plasmonic activity of the tip. Analysis of the signal decay allowed the authors to postulate a mechanism involving reactive decay chemistry of the photoexcited molecules with small molecules present in ambient (e.g., O_2).

The pristine environments achievable in UHV provide a means to mitigate photodissociation in pulsed-excitation TERS. Pozzi et al. subsequently used the same OPO described above to collect UHV-TERS of R6G using picosecond excitation.[208] Multimodal TERS was observed only with the tip in close proximity to the Ag(111) surface (Figure 16). Importantly, the signal was not observed to decay irreversibly as in ambient, but fluctuations in the signal intensity prevented kinetic analysis of the UHV-TER signal with continued irradiation. The authors determined the effects of UHV on signal persistence using SERS, wherein averaging over many hot spots reduces intensity fluctuations. Decay was slowed by a factor of 5 in UHV compared to ambient conditions. Amplifying signal decay using higher excitation intensity enabled a critical analysis of the decay mechanism, which was determined to be a result of surface diffusion of the R6G across the silver surface. While signal decay in pulsed excitation TERS can arise from photochemistry as well as surface diffusion, a UHV environment is clearly an asset.

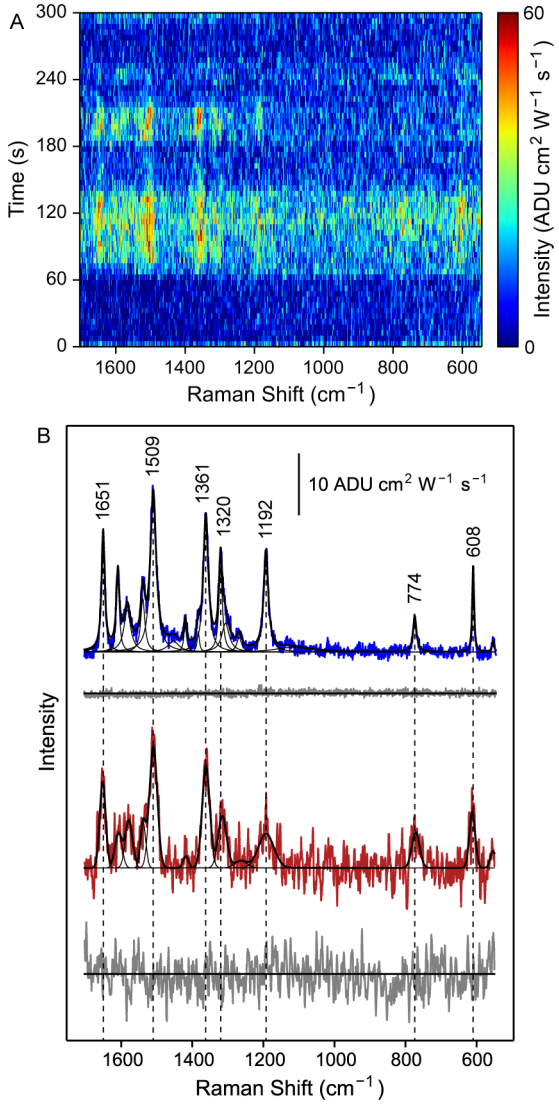

Figure 16. (A) Waterfall plot of 60 5 s TER spectra of R6G collected using 532 nm picosecond irradiation. Initially retracted Ag tip was brought into tunneling range at t = 60 s. (B) CW TER engaged (blue) and retracted (gray) spectra plotted above averaged picosecond spectra with the tip engaged (red) and retracted (gray) from A. Black lines represent individual and composite peak fits. Included scale bar applies to all plotted spectra. Reprinted with permission from ref 208. Copyright 2014 American Chemical Society.

Advances in ultrafast TERS have also been made using apparatuses operated in ambient. The Wickramasinghe group reported stimulated TERS of ABT on an evaporated Au film.[209] Here, the authors used a CW 632.8 nm laser to induce the Raman transition and aligned the energy of a 30 kHz diode laser to overlap with the 1142 cm^{-1} Stokes transition of ABT. This beam then stimulated the downward Raman transition corresponding to that particular vibrational mode. While stimulating only one mode sacrifices the chemical information contained in a full Raman spectrum, the authors reported an estimated stimulated gain of 1.0 × 10^9, thus increasing sensitivity compared to spontaneous TERS. Using this increased sensitivity, TER images were collected with the imaging rates limited not by TER signal strength but instead by the STM scanning rate. Using the ideas presented in this review, a pulsed Raman beam overlapped in time with the stimulating beam would allow stimulated TERS to resolve ultrafast dynamics of surface-bound molecules.

The Kawata group reported integration of TERS with a well-established nonlinear Raman technique, CARS. In initial TE-CARS experiments, individual modes of robust molecular systems, namely, adenine encased in DNA nanocrystals[210,211] and SWCNTs,[212] were probed with narrow band excitation from mode-locked Ti:sapphire lasers. Tip enhancement of the signal enabled samples to be imaged, and resulting optical images exhibited higher spatial resolution than topographic imaging, which was argued to be a result of the nonlinearity of the CARS process. Touched on in these reports is the inevitability of an electronic CARS signal arising from the third-order nonlinear susceptibility of Ag. This issue was not explored in depth but is an important consideration in any surface- or tip-enhanced CARS experiment. Later, a nominally broad-band variant of the technique applied to semiconducting carbon nanotubes (s-CNTs) was reported.[213] In this report, a delay between pulses allowed the kinetics of near-field signal decay to be discerned. While only one mode of the s-CNTs was visible in the collected spectra, the study serves as a proof-of-concept for future TE-CARS experiments using complete molecular vibrational fingerprints.

5. SUMMARY AND OUTLOOK

TERS has developed into a powerful and broadly versatile surface characterization method. It maintains the sensitivity of SERS while improving control of the enhancing field and increasing the breadth of compatible surfaces. Interest in the technique is widespread, as the number of groups utilizing TERS has grown appreciably. Concomitantly, multiple companies have commercialized TERS apparatuses. Using both commercial and homemade instruments, single-molecule investigations have become commonplace, with collected signals reporting not only the presence of each molecule but also a description of their internal structures and relevant environmental interactions. Lateral resolution down to roughly the size of the molecules under study has become possible,

DOI: 10.1021/acs.chemrev.6b00343
Chem. Rev. 2017, 117, 4961−4982

length scales at which the stability and cleanliness of UHV environments become increasingly beneficial.

Moving forward, increasing the reproducibility of tip fabrication and extending the applicability of TERS with respect to substrates and molecular systems will facilitate more pervasive use of TERS in the surface science community. The development of high-throughput and/or parallelized fabrication methods would be very advantageous and would be more amenable to commercial distribution at a reasonable price. The use of cleaning methods or coatings toward increasing the lifetime of tips has been discussed in the literature.[136,214] A universal and efficient method for cleaning or encapsulating Au and Ag tips would also do a great deal to increase the lifetime and reusability of fabricated probes.

While many TERS reports to date have focused on technique development using ideal probe molecules, advances have enabled research on more weakly scattering analytes. More complex systems will be studied, allowing direct applications of TERS to interfacial systems across an array of fields in science and engineering. UHV-TERS studies of nonresonant molecules could be achieved on well-defined substrates to evaluate substrate effects at step edges versus at terraces, for instance. Unfortunately, the scan rate of TERS mapping is currently limited by the integration time required at each point, but the identification of a new enhancement mechanism could speed up mapping or even allow SMTERS of nonresonant molecules. One possible avenue is the combination of stimulated Raman with UHV-TERS.[209] Fundamental research into the mechanisms of tip enhancement and the ultimate limit of lateral resolution are sure to continue, and the physics learned will help guide future TERS endeavors. In particular, resolution at or below 1 nm has only been demonstrated for a limited set of molecules. It will be of great interest to determine if this is a general mechanism and if it is limited to STM-TERS or if it can be achieved using AFM-TERS. In addition, efforts will focus on incorporating nonlinear spectroscopic approaches with TERS toward the goal of resolving the ultrafast dynamics of physical and chemical processes at the nanoscale.

AUTHOR INFORMATION

Corresponding Author

*E-mail: vanduyne@northwestern.edu.

ORCID

Craig T. Chapman: 0000-0001-5349-5359
Michael O. McAnally: 0000-0002-8681-2952
Mark C. Hersam: 0000-0003-4120-1426
Richard P. Van Duyne: 0000-0001-8861-2228

Notes

The authors declare no competing financial interest.

Biographies

Eric A. Pozzi studied Biochemistry, Chemistry, and Mathematics at the University of Colorado at Boulder and received his B.A. degree in 2011. At the University of Colorado he pursued high-pressure spectroscopic research of fluorescent protein variants under the advisement of J. Mathias Weber. He then joined the Department of Chemistry at Northwestern University and pursued research in the laboratories of Richard P. Van Duyne and Mark C. Hersam, graduating with his Ph.D. degree in 2016. At Northwestern, he investigated the physical and photophysical properties of surface-bound molecular species using ambient and ultrahigh-vacuum surface- and tip-enhanced Raman spectroscopies.

Guillaume Goubert obtained his B.S. degree in Optical Engineering (2008) at the Institute of Optics, Palaiseau (France), and his M.S. degree in Physics (2010) at Laval University, Quebec city (Canada). He received his Ph.D. degree in Chemistry (2014) at Laval University under the supervision of Prof. Peter McBreen studying asymmetric heterogeneous catalysis at the single-molecule level. He was awarded a NSERC postdoctoral fellowship in 2014 and is currently working in the laboratory of Prof. Richard P. Van Duyne at Northwestern University, where he focuses on studying electrochemistry at the nanoscale, combining Raman spectroscopy and scanning probe microscopy. His research interests include charge transfer at the nanoscale, heterogeneous catalysis, intermolecular interactions at surfaces, and nanoscale spectroscopy.

Naihao Chiang received his B.S. degrees in Chemistry, Physics, and Economics/Mathematics from the University of Southern California (USC) in 2010. He is currently a Ph.D. student in applied physics at Northwestern University under the supervision of Professor Richard P. Van Duyne and Tamar Seideman. His research interests focus on ultrahigh-vacuum tip-enhanced Raman spectroscopy and its applications.

Nan Jiang received his Ph.D. degree in Condensed Matter Physics from Chinese Academy of Sciences in 2010. Following postdoctoral studies at Northwestern University with Prof. Richard Van Duyne, in 2015 he joined the University of Illinois at Chicago as an assistant professor in the Department of Chemistry. His research focuses on developing imaging and spectroscopy technology to study physics and chemistry at the nanometer scale.

Craig T. Chapman received his Ph.D. degree in Chemistry from the University of Oregon in 2010 under the supervision of Jeffrey A. Cina, studying quantum dynamics and the theory of ultrafast nonlinear spectroscopy. He then performed postdoctoral research on the electronic structure and charge-transfer dynamics of fullerene derivatives with Xiaosong Li at the University of Washington. He is currently a postdoctoral fellow with George C. Schatz at Northwestern University. His research is concerned with the photoinduced dynamical properties of excitonic and plasmonic systems.

Michael O. McAnally received his B.S. degree in Chemistry and Mathematics from the University of Wisconsin—Eau Claire in 2011. He is currently pursuing his graduate work in the research groups of Richard P. Van Duyne and George C. Schatz groups at Northwestern University, focusing on developing novel plasmonically enhanced coherent Raman scattering experiments and theory. His current research interests include experimental studies of the molecule–plasmon coupling by correlated plasmonically enhanced coherent Raman scattering microscopy and localized surface plasmon resonance studies with semiclassical and quantum theoretical method development.

Anne-Isabelle Henry is a Research Assistant Professor at Northwestern University. She joined the Department of Chemistry after completing her doctoral thesis on the rational design and intrinsic properties of nanocrystal superlattices. She has extensive experience working with plasmonic nanomaterials—from their synthesis, assembly, and structure–function relationships to implementing strategies for harvesting their potential as optical sensors for defense and healthcare applications. Lately, her research has focused on the development of nanoplasmonic sensors for bioanalyte detection using SERS. She is also actively involved in managing research programs involving SERS biosensing and TERS-enabled nanoscale imaging. She received her B.S. (2002) and a M.S. (2004) degrees from University of Paris-Sud,

DOI: 10.1021/acs.chemrev.6b00343
Chem. Rev. 2017, 117, 4961–4982

France, and Ph.D. (2008) degree in Physical Chemistry (summa cum laude) from Pierre and Marie Curie University, France.

Tamar Seideman is a Professor of Chemistry and Physics at Northwestern. She received her Ph.D. degree in Chemical Physics from the Weizmann Institute, Israel, in 1989. Her research interests include quantum transport, molecular electronics, current-driven nanochemistry and molecular machines, nanoplasmonics and light manipulation in the nanoscale, coherent control and coherence spectroscopies in isolated molecules and in dissipative media, the interaction of matter with intense laser fields, photomanipulation of external and internal molecular modes, and mathematical method development.

George C. Schatz is the Morrison Professor of Chemistry and Professor of Chemical and Biological Engineering at Northwestern University. He received his B.S. degree from Clarkson University (1971) and Ph.D. degree from Caltech (1976). He is a member of the National Academy of Sciences and the American Academy of Arts and Sciences. His research broadly covers theory as applied to nanomaterials and biomaterials.

Mark C. Hersam is the Walter P. Murphy Professor of Materials Science and Engineering and Director of the Materials Research Center at Northwestern University. He earned a B.S. degree in Electrical Engineering from the University of Illinois at Urbana—Champaign (UIUC) in 1996, M.Phil. degree in Physics from the University of Cambridge in 1997, and Ph.D. degree in Electrical Engineering from UIUC in 2000. His research interests include nanofabrication, scanning probe microscopy, semiconductor surfaces, and nanoelectronic materials. His work has been recognized with several awards including a Presidential Early Career Award for Scientists and Engineers and a MacArthur Fellowship.

Richard P. Van Duyne is the Charles E. and Emma H. Morrison Professor of Chemistry and of Biomedical Engineering at Northwestern University. He received his B.S. degree (1967) at Rensselaer Polytechnic Institute and Ph.D. degree (1971) at the University of North Carolina, Chapel Hill, both in Chemistry. He is a member of the National Academy of Sciences and the American Academy of Arts and Sciences. He is known for the discovery of surface-enhanced Raman spectroscopy (SERS), the invention of nanosphere lithography (NSL), and development of ultrasensitive nanosensors based on localized surface plasmon resonance (LSPR) spectroscopy.

ACKNOWLEDGMENTS

E.A.P., C.T.C., M.O.M., G.C.S., and R.P.V.D. acknowledge support from the National Science Foundation Center for Chemical Innovation dedicated to Chemistry at the Space—Time Limit (CaSTL), Grant CHE-1414466. G.G., A.-I.H., and R.P.V.D were supported by the Air Force Office of Scientific Research MURI (FA9550-14-1-0003). N.C., N.J., T.S., M.C.H., and R.P.V.D. acknowledge funding from the Department of Energy Office of Basic Energy Sciences (SISGR Grant DE-FG02-09ER16109). E.A.P., G.C.S., M.C.H., and R.P.V.D. also acknowledge support from the National Science Foundation Materials Research Science and Engineering Center (DMR-1121262). E.A.P. and M.O.M. were additionally supported by the National Science Foundation Graduate Research Fellowship under Grant DGE-1324585.

REFERENCES

(1) Moore, G. E. Progress in Digital Integrated Electronics. *Proceedings of the IEEE International Electron Devices Meeting*, Washington D.C., 1975; IEEE, 1975; pp 11—13.
(2) Heath, J. R.; Ratner, M. A. Molecular Electronics. *Phys. Today* **2003**, *56*, 43—49.
(3) Somorjai, G. A. The Surface Science of Heterogeneous Catalysis. *Surf. Sci.* **1994**, *299-300*, 849—866.
(4) Poudel, B.; Hao, Q.; Ma, Y.; Lan, Y.; Minnich, A.; Yu, B.; Yan, X.; Wang, D.; Muto, A.; Vashaee, D.; et al. High-Thermoelectric Performance of Nanostructured Bismuth Antimony Telluride Bulk Alloys. *Science* **2008**, *320*, 634—638.
(5) Lu, K.; Lu, L.; Suresh, S. Strengthening Materials by Engineering Coherent Internal Boundaries at the Nanoscale. *Science* **2009**, *324*, 349—352.
(6) Gleiter, H. Nanostructured Materials: Basic Concepts and Microstructure. *Acta Mater.* **2000**, *48*, 1—29.
(7) Bell, A. T. The Impact of Nanoscience on Heterogeneous Catalysis. *Science* **2003**, *299*, 1688—1691.
(8) Lauritsen, J. V.; Kibsgaard, J.; Helveg, S.; Topsøe, H.; Clausen, B. S.; Lægsgaard, E.; Besenbacher, F. Size-Dependent Structure of MoS2 Nanocrystals. *Nat. Nanotechnol.* **2007**, *2*, 53—58.
(9) Lai, X.; Goodman, D. W. Structure—Reactivity Correlations for Oxide-Supported Metal Catalysts: New Perspectives from STM. *J. Mol. Catal. A: Chem.* **2000**, *162*, 33—50.
(10) Hörber, J. K. H.; Miles, M. J. Scanning Probe Evolution in Biology. *Science* **2003**, *302*, 1002—1005.
(11) Loos, J. The Art of SPM: Scanning Probe Microscopy in Materials Science. *Adv. Mater.* **2005**, *17*, 1821—1833.
(12) Müller, D. J.; Dufrene, Y. F. Atomic Force Microscopy as a Multifunctional Molecular Toolbox in Nanobiotechnology. *Nat. Nanotechnol.* **2008**, *3*, 261—269.
(13) Yoshimoto, S.; Itaya, K. Adsorption and Assembly of Ions and Organic Molecules at Electrochemical Interfaces: Nanoscale Aspects. *Annu. Rev. Anal. Chem.* **2013**, *6*, 213—235.
(14) Repp, J.; Meyer, G.; Stojković, S. M.; Gourdon, A.; Joachim, C. Molecules on Insulating Films: Scanning-Tunneling Microscopy Imaging of Individual Molecular Orbitals. *Phys. Rev. Lett.* **2005**, *94*, 026803.
(15) de Oteyza, D. G.; Gorman, P.; Chen, Y.-C.; Wickenburg, S.; Riss, A.; Mowbray, D. J.; Etkin, G.; Pedramrazi, Z.; Tsai, H.-Z.; Rubio, A.; et al. Direct Imaging of Covalent Bond Structure in Single-Molecule Chemical Reactions. *Science* **2013**, *340*, 1434—1437.
(16) Hansma, P. K.; Tersoff, J. Scanning Tunneling Microscopy. *J. Appl. Phys.* **1987**, *61*, R1—R24.
(17) Gimzewski, J. K.; Möller, R. Transition from the Tunneling Regime to Point Contact Studied Using Scanning Tunneling Microscopy. *Phys. Rev. B: Condens. Matter Mater. Phys.* **1987**, *36*, 1284—1287.
(18) Thompson, R. E.; Larson, D. R.; Webb, W. W. Precise Nanometer Localization Analysis for Individual Fluorescent Probes. *Biophys. J.* **2002**, *82*, 2775—2783.
(19) Willets, K. A.; Stranahan, S. M.; Weber, M. L. Shedding Light on Surface-Enhanced Raman Scattering Hot Spots through Single-Molecule Super-Resolution Imaging. *J. Phys. Chem. Lett.* **2012**, *3*, 1286—1294.
(20) Hell, S. W. Far-Field Optical Nanoscopy. *Science* **2007**, *316*, 1153—1158.
(21) Huang, B.; Wang, W.; Bates, M.; Zhuang, X. Three-Dimensional Super-Resolution Imaging by Stochastic Optical Reconstruction Microscopy. *Science* **2008**, *319*, 810—813.
(22) Biteen, J. S.; Thompson, M. A.; Tselentis, N. K.; Bowman, G. R.; Shapiro, L.; Moerner, W. E. Super-Resolution Imaging in Live Caulobacter Crescentus Cells Using Photoswitchable EYFP. *Nat. Methods* **2008**, *5*, 947—949.
(23) Pavliček, N.; Schuler, B.; Collazos, S.; Moll, N.; Pérez, D.; Guitián, E.; Meyer, G.; Peña, D.; Gross, L. On-Surface Generation and Imaging of Arynes by Atomic Force Microscopy. *Nat. Chem.* **2015**, *7*, 623—628.
(24) Ho, W. Single-Molecule Chemistry. *J. Chem. Phys.* **2002**, *117*, 11033—11061.

DOI: 10.1021/acs.chemrev.6b00343
Chem. Rev. 2017, 117, 4961—4982

(25) Hipps, K. W.; Mazur, U. Inelastic Electron Tunneling: An Alternative Molecular Spectroscopy. *J. Phys. Chem.* **1993**, *97*, 7803−7814.
(26) Guo, J.; Lü, J.-T.; Feng, Y.; Chen, J.; Peng, J.; Lin, Z.; Meng, X.; Wang, Z.; Li, X.-Z.; Wang, E.-G. Nuclear Quantum Effects of Hydrogen Bonds Probed by Tip-Enhanced Inelastic Electron Tunneling. *Science* **2016**, *352*, 321−325.
(27) Nilsson, A.; Pettersson, L. G. M. Chemical Bonding on Surfaces Probed by X-Ray Emission Spectroscopy and Density Functional Theory. *Surf. Sci. Rep.* **2004**, *55*, 49−167.
(28) Lee, P. A.; Citrin, P. H.; Eisenberger, P.; Kincaid, B. M. Extended X-Ray Absorption Fine Structure—Its Strengths and Limitations as a Structural Tool. *Rev. Mod. Phys.* **1981**, *53*, 769−806.
(29) Bergmann, U.; Glatzel, P.; Cramer, S. P. Bulk-Sensitive XAS Characterization of Light Elements: From X-Ray Raman Scattering to X-Ray Raman Spectroscopy. *Microchem. J.* **2002**, *71*, 221−230.
(30) Heald, S. M. EXAFS at Grazing Incidence: Data Collection and Analysis. *Rev. Sci. Instrum.* **1992**, *63*, 873−878.
(31) Pozzi, E. A.; Zrimsek, A. B.; Lethiec, C. M.; Schatz, G. C.; Hersam, M. C.; Van Duyne, R. P. Evaluating Single-Molecule Stokes and Anti-Stokes SERS for Nanoscale Thermometry. *J. Phys. Chem. C* **2015**, *119*, 21116−21124.
(32) Balois, M. V.; Hayazawa, N.; Catalan, F. C.; Kawata, S.; Yano, T.; Hayashi, T. Tip-Enhanced THz Raman Spectroscopy for Local Temperature Determination at the Nanoscale. *Anal. Bioanal. Chem.* **2015**, *407*, 8205−8213.
(33) Dieringer, J. A.; McFarland, A. D.; Shah, N. C.; Stuart, D. A.; Whitney, A. V.; Yonzon, C. R.; Young, M. A.; Zhang, X.; Van Duyne, R. P. Introductory Lecture Surface Enhanced Raman Spectroscopy: New Materials, Concepts, Characterization Tools, and Applications. *Faraday Discuss.* **2006**, *132*, 9−26.
(34) Moerner, W. E.; Kador, L. Optical Detection and Spectroscopy of Single Molecules in a Solid. *Phys. Rev. Lett.* **1989**, *62*, 2535−2538.
(35) Orrit, M.; Bernard, J. Single Pentacene Molecules Detected by Fluorescence Excitation in a p-Terphenyl Crystal. *Phys. Rev. Lett.* **1990**, *65*, 2716−2719.
(36) Ayuyan, A. G.; Cohen, F. S. Lipid Peroxides Promote Large Rafts: Effects of Excitation of Probes in Fluorescence Microscopy and Electrochemical Reactions During Vesicle Formation. *Biophys. J.* **2006**, *91*, 2172−2183.
(37) Dickson, R. M.; Cubitt, A. B.; Tsien, R. Y.; Moerner, W. E. On/Off Blinking and Switching Behaviour of Single Molecules of Green Fluorescent Protein. *Nature* **1997**, *388*, 355−358.
(38) Sannomiya, T.; Hafner, C.; Voros, J. In Situ Sensing of Single Binding Events by Localized Surface Plasmon Resonance. *Nano Lett.* **2008**, *8*, 3450−3455.
(39) Chen, S.; Svedendahl, M.; Van Duyne, R. P.; Käll, M. Plasmon-Enhanced Colorimetric ELISA with Single Molecule Sensitivity. *Nano Lett.* **2011**, *11*, 1826−1830.
(40) Ament, I.; Prasad, J.; Henkel, A.; Schmachtel, S.; Sönnichsen, C. Single Unlabeled Protein Detection on Individual Plasmonic Nanoparticles. *Nano Lett.* **2012**, *12*, 1092−1095.
(41) Zijlstra, P.; Paulo, P. M. R.; Orrit, M. Optical Detection of Single Non-Absorbing Molecules Using the Surface Plasmon Resonance of a Gold Nanorod. *Nat. Nanotechnol.* **2012**, *7*, 379−382.
(42) Langelüddecke, L.; Singh, P.; Deckert, V. Exploring the Nanoscale: Fifteen Years of Tip-Enhanced Raman Spectroscopy. *Appl. Spectrosc.* **2015**, *69*, 1357−1371.
(43) Mauser, N.; Hartschuh, A. Tip-Enhanced Near-Field Optical Microscopy. *Chem. Soc. Rev.* **2014**, *43*, 1248−1262.
(44) Schmid, T.; Opilik, L.; Blum, C.; Zenobi, R. Nanoscale Chemical Imaging Using Tip-Enhanced Raman Spectroscopy: A Critical Review. *Angew. Chem., Int. Ed.* **2013**, *52*, 5940−5954.
(45) Pettinger, B.; Schambach, P.; Villagómez, C. J.; Scott, N. Tip-Enhanced Raman Spectroscopy: Near-Fields Acting on a Few Molecules. *Annu. Rev. Phys. Chem.* **2012**, *63*, 379−399.
(46) Lucas, M.; Riedo, E. Invited Review Article: Combining Scanning Probe Microscopy with Optical Spectroscopy for Applications in Biology and Materials Science. *Rev. Sci. Instrum.* **2012**, *83*, 061101.
(47) Zhang, C.; Chen, L.; Zhang, R.; Dong, Z. Scanning Tunneling Microscope Based Nanoscale Optical Imaging of Molecules on Surfaces. *Jpn. J. Appl. Phys.* **2015**, *54*, 08LA01.
(48) Kumar, N.; Mignuzzi, S.; Su, W.; Roy, D. Tip-Enhanced Raman Spectroscopy: Principles and Applications. *EPJ. Technol. Instrum.* **2015**, *2*, 1−23.
(49) Schultz, Z. D.; Marr, J. M.; Wang, H. Tip Enhanced Raman Scattering: Plasmonic Enhancements for Nanoscale Chemical Analysis. *Nanophotonics* **2014**, *3*, 91−104.
(50) Sun, M.; Zhang, Z.; Chen, L.; Sheng, S.; Xu, H. Plasmonic Gradient Effects on High Vacuum Tip-Enhanced Raman Spectroscopy. *Adv. Opt. Mater.* **2014**, *2*, 74−80.
(51) Sonntag, M. D.; Klingsporn, J. M.; Zrimsek, A. B.; Sharma, B.; Ruvuna, L. K.; Van Duyne, R. P. Molecular Plasmonics for Nanoscale Spectroscopy. *Chem. Soc. Rev.* **2014**, *43*, 1230−1247.
(52) Sharma, B.; Frontiera, R. R.; Henry, A.-I.; Ringe, E.; Van Duyne, R. P. SERS: Materials, Applications, and the Future. *Mater. Today* **2012**, *15*, 16−25.
(53) Le Ru, E. C.; Etchegoin, P. G. Single-Molecule Surface-Enhanced Raman Spectroscopy. *Annu. Rev. Phys. Chem.* **2012**, *63*, 65−87.
(54) Schlücker, S. Surface-Enhanced Raman Spectroscopy: Concepts and Chemical Applications. *Angew. Chem., Int. Ed.* **2014**, *53*, 4756−4795.
(55) Cialla, D.; März, A.; Böhme, R.; Theil, F.; Weber, K.; Schmitt, M.; Popp, J. Surface-Enhanced Raman Spectroscopy (SERS): Progress and Trends. *Anal. Bioanal. Chem.* **2012**, *403*, 27−54.
(56) Fleischmann, M.; Hendra, P. J.; McQuillan, A. J. Raman Spectra of Pyridine Adsorbed at a Silver Electrode. *Chem. Phys. Lett.* **1974**, *26*, 163−166.
(57) Jeanmaire, D. L.; Van Duyne, R. P. Surface Raman Spectroelectrochemistry: Part I. Heterocyclic, Aromatic, and Aliphatic Amines Adsorbed on the Anodized Silver Electrode. *J. Electroanal. Chem. Interfacial Electrochem.* **1977**, *84*, 1−20.
(58) Albrecht, M. G.; Creighton, J. A. Anomalously Intense Raman Spectra of Pyridine at a Silver Electrode. *J. Am. Chem. Soc.* **1977**, *99*, 5215−5217.
(59) Moskovits, M. Surface-Enhanced Spectroscopy. *Rev. Mod. Phys.* **1985**, *57*, 783−826.
(60) Nie, S.; Emory, S. R. Probing Single Molecules and Single Nanoparticles by Surface-Enhanced Raman Scattering. *Science* **1997**, *275*, 1102−1106.
(61) Kneipp, K.; Wang, Y.; Kneipp, H.; Perelman, L. T.; Itzkan, I.; Dasari, R. R.; Feld, M. S. Single Molecule Detection Using Surface-Enhanced Raman Scattering (SERS). *Phys. Rev. Lett.* **1997**, *78*, 1667−1670.
(62) Le Ru, E. C.; Meyer, M.; Etchegoin, P. G. Proof of Single-Molecule Sensitivity in Surface Enhanced Raman Scattering (SERS) by Means of a Two-Analyte Technique. *J. Phys. Chem. B* **2006**, *110*, 1944−1948.
(63) Le Ru, E. C.; Blackie, E.; Meyer, M.; Etchegoin, P. G. Surface Enhanced Raman Scattering Enhancement Factors: A Comprehensive Study. *J. Phys. Chem. C* **2007**, *111*, 13794−13803.
(64) Goulet, P. J. G.; Aroca, R. F. Distinguishing Individual Vibrational Fingerprints: Single-Molecule Surface-Enhanced Resonance Raman Scattering from One-to-One Binary Mixtures in Langmuir-Blodgett Monolayers. *Anal. Chem.* **2007**, *79*, 2728−2734.
(65) Etchegoin, P. G.; Meyer, M.; Blackie, E.; Le Ru, E. C. Statistics of Single-Molecule Surface Enhanced Raman Scattering Signals: Fluctuation Analysis with Multiple Analyte Techniques. *Anal. Chem.* **2007**, *79*, 8411−8415.
(66) Domke, K. F.; Zhang, D.; Pettinger, B. Enhanced Raman Spectroscopy: Single Molecules or Carbon? *J. Phys. Chem. C* **2007**, *111*, 8611−8616.
(67) Zrimsek, A. B.; Wong, N. L.; Van Duyne, R. P. Single Molecule Surface-Enhanced Raman Spectroscopy: A Critical Analysis of the

DOI: 10.1021/acs.chemrev.6b00343
Chem. Rev. 2017, 117, 4961−4982

Bianalyte Versus Isotopologue Proof. *J. Phys. Chem. C* **2016**, *120*, 5133−5142.
(68) Dieringer, J. A.; Lettan, R. B.; Scheidt, K. A.; Van Duyne, R. P. A Frequency Domain Existence Proof of Single-Molecule Surface-Enhanced Raman Spectroscopy. *J. Am. Chem. Soc.* **2007**, *129*, 16249−16256.
(69) Kleinman, S. L.; Ringe, E.; Valley, N.; Wustholz, K. L.; Phillips, E.; Scheidt, K. A.; Schatz, G. C.; Van Duyne, R. P. Single-Molecule Surface-Enhanced Raman Spectroscopy of Crystal Violet Isotopologues: Theory and Experiment. *J. Am. Chem. Soc.* **2011**, *133*, 4115−4122.
(70) Etchegoin, P. G.; Le Ru, E. C.; Meyer, M. Evidence of Natural Isotopic Distribution from Single-Molecule SERS. *J. Am. Chem. Soc.* **2009**, *131*, 2713−2716.
(71) Wang, D.; Zhu, W.; Best, M. D.; Camden, J. P.; Crozier, K. B. Directional Raman Scattering from Single Molecules in the Feed Gaps of Optical Antennas. *Nano Lett.* **2013**, *13*, 2194−2198.
(72) Zrimsek, A. B.; Henry, A.-I.; Van Duyne, R. P. Single Molecule Surface-Enhanced Raman Spectroscopy without Nanogaps. *J. Phys. Chem. Lett.* **2013**, *4*, 3206−3210.
(73) Gersten, J. I.; Nitzan, A. Electromagnetic Theory of Enhanced Raman Scattering by Molecules Adsorbed on Rough Surfaces. *J. Chem. Phys.* **1980**, *73*, 3023−3037.
(74) Wang, D.-S.; Chew, H.; Kerker, M. Enhanced Raman Scattering at the Surface (SERS) of a Spherical Particle. *Appl. Opt.* **1980**, *19*, 2256−2257.
(75) Billmann, J.; Otto, A. Electronic Surface State Contribution to Surface Enhanced Raman Scattering. *Solid State Commun.* **1982**, *44*, 105−107.
(76) Schatz, G. C.; Van Duyne, R. P. In *Handbook of Vibrational Spectroscopy*; Chalmers, J. M., Griffiths, P. R., Ed.; Wiley: New York, 2002; Vol. *1*, pp 759−774.
(77) Murray, C. A.; Allara, D. L. Measurement of the Molecule-Silver Separation Dependence of Surface Enhanced Raman Scattering in Multilayered Structures. *J. Chem. Phys.* **1982**, *76*, 1290−1303.
(78) Weitz, D. A.; Gramila, T. J.; Genack, A. Z.; Gersten, J. I. Anomalous Low-Frequency Raman Scattering from Rough Metal Surfaces and the Origin of Surface-Enhanced Raman Scattering. *Phys. Rev. Lett.* **1980**, *45*, 355−358.
(79) Weitz, D. A.; Garoff, S.; Gersten, J. I.; Nitzan, A. The Enhancement of Raman Scattering, Resonance Raman Scattering, and Fluorescence from Molecules Adsorbed on a Rough Silver Surface. *J. Chem. Phys.* **1983**, *78*, 5324−5338.
(80) Schatz, G. C.; Young, M. A.; Van Duyne, R. P. In *Surface-Enhanced Raman Scattering*; Kneipp, K., Moskovits, M., Kneipp, H., Eds.; Springer: Berlin, 2006; Vol. *103*, pp 19−46.
(81) Campion, A.; Ivanecky, J. E., III; Child, C. M.; Foster, M. On the Mechanism of Chemical Enhancement in Surface-Enhanced Raman Scattering. *J. Am. Chem. Soc.* **1995**, *117*, 11807−11808.
(82) Moore, J. E.; Morton, S. M.; Jensen, L. Importance of Correctly Describing Charge-Transfer Excitations for Understanding the Chemical Effect in SERS. *J. Phys. Chem. Lett.* **2012**, *3*, 2470−2475.
(83) Morton, S. M.; Jensen, L. Understanding the Molecule−Surface Chemical Coupling in SERS. *J. Am. Chem. Soc.* **2009**, *131*, 4090−4098.
(84) Morton, S. M.; Ewusi-Annan, E.; Jensen, L. Controlling the Non-Resonant Chemical Mechanism of SERS Using a Molecular Photoswitch. *Phys. Chem. Chem. Phys.* **2009**, *11*, 7424−7429.
(85) Stranahan, S. M.; Willets, K. A. Super-Resolution Optical Imaging of Single-Molecule SERS Hot Spots. *Nano Lett.* **2010**, *10*, 3777−3784.
(86) Cang, H.; Labno, A.; Lu, C.; Yin, X.; Liu, M.; Gladden, C.; Liu, Y.; Zhang, X. Probing the Electromagnetic Field of a 15-Nanometre Hotspot by Single Molecule Imaging. *Nature* **2011**, *469*, 385−388.
(87) Huang, T.; Xu, X.-H. N. Multicolored Nanometre-Resolution Mapping of Single Protein−Ligand Binding Complexes Using Far-Field Photostable Optical Nanoscopy (PHOTON). *Nanoscale* **2011**, *3*, 3567−3572.
(88) Weber, M. L.; Willets, K. A. Correlated Super-Resolution Optical and Structural Studies of Surface-Enhanced Raman Scattering Hot Spots in Silver Colloid Aggregates. *J. Phys. Chem. Lett.* **2011**, *2*, 1766−1770.
(89) Titus, E. J.; Weber, M. L.; Stranahan, S. M.; Willets, K. A. Super-Resolution SERS Imaging Beyond the Single-Molecule Limit: An Isotope-Edited Approach. *Nano Lett.* **2012**, *12*, 5103−5110.
(90) Olson, A. P.; Ertsgaard, C. T.; Elliott, S. N.; Lindquist, N. C. Super-Resolution Chemical Imaging with Plasmonic Substrates. *ACS Photonics* **2016**, *3*, 329−336.
(91) Hecht, B.; Sick, B.; Wild, U. P.; Deckert, V.; Zenobi, R.; Martin, O. J. F.; Pohl, D. W. Scanning Near-Field Optical Microscopy with Aperture Probes: Fundamentals and Applications. *J. Chem. Phys.* **2000**, *112*, 7761−7774.
(92) Deckert, V.; Zeisel, D.; Zenobi, R.; Vo-Dinh, T. Near-Field Surface-Enhanced Raman Imaging of Dye-Labeled DNA with 100-nm Resolution. *Anal. Chem.* **1998**, *70*, 2646−2650.
(93) Stöckle, R. M.; Deckert, V.; Fokas, C.; Zeisel, D.; Zenobi, R. Sub-Wavelength Raman Spectroscopy on Isolated Silver Islands. *Vib. Spectrosc.* **2000**, *22*, 39−48.
(94) Fokas, C.; Deckert, V. Towards in Situ Raman Microscopy of Single Catalytic Sites. *Appl. Spectrosc.* **2002**, *56*, 192−199.
(95) Wessel, J. Surface-Enhanced Optical Microscopy. *J. Opt. Soc. Am. B* **1985**, *2*, 1538−1541.
(96) Stöckle, R. M.; Suh, Y. D.; Deckert, V.; Zenobi, R. Nanoscale Chemical Analysis by Tip-Enhanced Raman Spectroscopy. *Chem. Phys. Lett.* **2000**, *318*, 131−136.
(97) Anderson, M. S. Locally Enhanced Raman Spectroscopy with an Atomic Force Microscope. *Appl. Phys. Lett.* **2000**, *76*, 3130−3132.
(98) Hayazawa, N.; Inouye, Y.; Sekkat, Z.; Kawata, S. Metallized Tip Amplification of Near-Field Raman Scattering. *Opt. Commun.* **2000**, *183*, 333−336.
(99) Pettinger, B.; Picardi, G.; Schuster, R.; Ertl, G. Surface Enhanced Raman Spectroscopy: Towards Single Molecule Spectroscopy. *Electrochemistry (Tokyo, Jpn.)* **2000**, *68*, 942−949.
(100) Anderson, M. S.; Pike, W. T. A Raman-Atomic Force Microscope for Apertureless-Near-Field Spectroscopy and Optical Trapping. *Rev. Sci. Instrum.* **2002**, *73*, 1198−1203.
(101) Hayazawa, N.; Tarun, A.; Inouye, Y.; Kawata, S. Near-Field Enhanced Raman Spectroscopy Using Side Illumination Optics. *J. Appl. Phys.* **2002**, *92*, 6983−6986.
(102) Pettinger, B.; Ren, B.; Picardi, G.; Schuster, R.; Ertl, G. Nanoscale Probing of Adsorbed Species by Tip-Enhanced Raman Spectroscopy. *Phys. Rev. Lett.* **2004**, *92*, 096101.
(103) Mehtani, D.; Lee, N.; Hartschuh, R. D.; Kisliuk, A.; Foster, M. D.; Sokolov, A. P.; Maguire, J. F. Nano-Raman Spectroscopy with Side-Illumination Optics. *J. Raman Spectrosc.* **2005**, *36*, 1068−1075.
(104) Stadler, J.; Schmid, T.; Zenobi, R. Developments in and Practical Guidelines for Tip-Enhanced Raman Spectroscopy. *Nanoscale* **2012**, *4*, 1856−1870.
(105) Steidtner, J.; Pettinger, B. High-Resolution Microscope for Tip-Enhanced Optical Processes in Ultrahigh Vacuum. *Rev. Sci. Instrum.* **2007**, *78*, 103104.
(106) Stanciu, C.; Sackrow, M.; Meixner, A. J. High NA Particle-and Tip-Enhanced Nanoscale Raman Spectroscopy with a Parabolic-Mirror Microscope. *J. Microsc.* **2008**, *229*, 247−253.
(107) Sun, M.; Zhang, Z.; Chen, L.; Li, Q.; Sheng, S.; Xu, H.; Song, P. Plasmon-Driven Selective Reductions Revealed by Tip-Enhanced Raman Spectroscopy. *Adv. Mater. Interfaces* **2014**, *1*, 1300125.
(108) Zhang, R.; Zhang, Y.; Dong, Z. C.; Jiang, S.; Zhang, C.; Chen, L. G.; Zhang, L.; Liao, Y.; Aizpurua, J.; Luo, Y.; et al. Chemical Mapping of a Single Molecule by Plasmon-Enhanced Raman Scattering. *Nature* **2013**, *498*, 82−86.
(109) Jiang, S.; Zhang, Y.; Zhang, R.; Hu, C.; Liao, M.; Luo, Y.; Yang, J.; Dong, Z.; Hou, J. G. Distinguishing Adjacent Molecules on a Surface Using Plasmon-Enhanced Raman Scattering. *Nat. Nanotechnol.* **2015**, *10*, 865−846.
(110) Chiang, N.; Jiang, N.; Chulhai, D. V.; Pozzi, E. A.; Hersam, M. C.; Jensen, L.; Seideman, T.; Van Duyne, R. P. Molecular-Resolution Interrogation of a Porphyrin Monolayer by Ultrahigh Vacuum Tip-

DOI: 10.1021/acs.chemrev.6b00343
Chem. Rev. 2017, 117, 4961−4982

Enhanced Raman and Fluorescence Spectroscopy. *Nano Lett.* **2015**, *15*, 4114−4120.
(111) Jiang, N.; Chiang, N.; Madison, L. R.; Pozzi, E. A.; Wasielewski, M. R.; Seideman, T.; Schatz, G. C.; Hersam, M. C.; Van Duyne, R. P. Nanoscale Chemical Imaging of a Dynamic Molecular Phase Boundary with Ultrahigh Vacuum Tip-Enhanced Raman Spectroscopy. *Nano Lett.* **2016**, *16*, 3898−3904.
(112) Hartschuh, A.; Sánchez, E. J.; Xie, X. S.; Novotny, L. High-Resolution Near-Field Raman Microscopy of Single-Walled Carbon Nanotubes. *Phys. Rev. Lett.* **2003**, *90*, 095503.
(113) Neacsu, C. C.; Dreyer, J.; Behr, N.; Raschke, M. B. Scanning-Probe Raman Spectroscopy with Single-Molecule Sensitivity. *Phys. Rev. B: Condens. Matter Mater. Phys.* **2006**, *73*, 193406.
(114) Zhang, W.; Yeo, B. S.; Schmid, T.; Zenobi, R. Single Molecule Tip-Enhanced Raman Spectroscopy with Silver Tips. *J. Phys. Chem. C* **2007**, *111*, 1733−1738.
(115) Liu, Z.; Ding, S.-Y.; Chen, Z.-B.; Wang, X.; Tian, J.-H.; Anema, J. R.; Zhou, X.-S.; Wu, D.-Y.; Mao, B.-W.; Xu, X.; et al. Revealing the Molecular Structure of Single-Molecule Junctions in Different Conductance States by Fishing-Mode Tip-Enhanced Raman Spectroscopy. *Nat. Commun.* **2011**, *2*, 305.
(116) Steidtner, J.; Pettinger, B. Tip-Enhanced Raman Spectroscopy and Microscopy on Single Dye Molecules with 15 nm Resolution. *Phys. Rev. Lett.* **2008**, *100*, 236101.
(117) Sonntag, M. D.; Klingsporn, J. M.; Garibay, L. K.; Roberts, J. M.; Dieringer, J. A.; Seideman, T.; Scheidt, K. A.; Jensen, L.; Schatz, G. C.; Van Duyne, R. P. Single-Molecule Tip-Enhanced Raman Spectroscopy. *J. Phys. Chem. C* **2012**, *116*, 478−483.
(118) Pettinger, B.; Domke, K. F.; Zhang, D.; Picardi, G.; Schuster, R. Tip-Enhanced Raman Scattering: Influence of the Tip-Surface Geometry on Optical Resonance and Enhancement. *Surf. Sci.* **2009**, *603*, 1335−1341.
(119) Sukharev, M.; Seideman, T. Optical Properties of Metal Tips for Tip-Enhanced Spectroscopies. *J. Phys. Chem. A* **2009**, *113*, 7508−7513.
(120) Pettinger, B. Single-Molecule Surface- and Tip-Enhanced Raman Spectroscopy. *Mol. Phys.* **2010**, *108*, 2039−2059.
(121) Micic, M.; Klymyshyn, N.; Suh, Y. D.; Lu, H. P. Finite Element Method Simulation of the Field Distribution for AFM Tip-Enhanced Surface-Enhanced Raman Scanning Microscopy. *J. Phys. Chem. B* **2003**, *107*, 1574−1584.
(122) Yang, Z.; Aizpurua, J.; Xu, H. Electromagnetic Field Enhancement in TERS Configurations. *J. Raman Spectrosc.* **2009**, *40*, 1343−1348.
(123) Downes, A.; Salter, D.; Elfick, A. Finite Element Simulations of Tip-Enhanced Raman and Fluorescence Spectroscopy. *J. Phys. Chem. B* **2006**, *110*, 6692−6698.
(124) Angulo, A. M.; Noguez, C.; Schatz, G. C. Electromagnetic Field Enhancement for Wedge-Shaped Metal Nanostructures. *J. Phys. Chem. Lett.* **2011**, *2*, 1978−1983.
(125) Kazemi-Zanjani, N.; Vedraine, S.; Lagugné-Labarthet, F. Localized Enhancement of Electric Field in Tip-Enhanced Raman Spectroscopy Using Radially and Linearly Polarized Light. *Opt. Express* **2013**, *21*, 25271−25276.
(126) Meng, L.; Huang, T.; Wang, X.; Chen, S.; Yang, Z.; Ren, B. Gold-Coated AFM Tips for Tip-Enhanced Raman Spectroscopy: Theoretical Calculation and Experimental Demonstration. *Opt. Express* **2015**, *23*, 13804−13813.
(127) Ausman, L. K.; Schatz, G. C. On the Importance of Incorporating Dipole Reradiation in the Modeling of Surface Enhanced Raman Scattering from Spheres. *J. Chem. Phys.* **2009**, *131*, 084708.
(128) Pettinger, B.; Picardi, G.; Schuster, R.; Ertl, G. Surface-Enhanced and STM Tip-Enhanced Raman Spectroscopy of CN− Ions at Gold Surfaces. *J. Electroanal. Chem.* **2003**, *554-555*, 293−299.
(129) Pettinger, B.; Ren, B.; Picardi, G.; Schuster, R.; Ertl, G. Tip-Enhanced Raman Spectroscopy (TERS) of Malachite Green Isothiocyanate at Au(111): Bleaching Behavior under the Influence of High Electromagnetic Fields. *J. Raman Spectrosc.* **2005**, *36*, 541−550.
(130) Roy, D.; Wang, J.; Williams, C. Novel Methodology for Estimating the Enhancement Factor for Tip-Enhanced Raman Spectroscopy. *J. Appl. Phys.* **2009**, *105*, 013530.
(131) Stadler, J.; Schmid, T.; Zenobi, R. Nanoscale Chemical Imaging Using Top-Illumination Tip-Enhanced Raman Spectroscopy. *Nano Lett.* **2010**, *10*, 4514−4520.
(132) Stiles, P. L.; Dieringer, J. A.; Shah, N. C.; Van Duyne, R. P. Surface-Enhanced Raman Spectroscopy. *Annu. Rev. Anal. Chem.* **2008**, *1*, 601−626.
(133) McCreery, R. L. *Raman Spectroscopy for Chemical Analysis*; John Wiley & Sons: New York, 2000.
(134) Albrecht, A. C.; Hutley, M. C. On the Dependence of Vibrational Raman Intensity on the Wavelength of Incident Light. *J. Chem. Phys.* **1971**, *55*, 4438−4443.
(135) Zhao, J.; Dieringer, J. A.; Zhang, X.; Schatz, G. C.; Van Duyne, R. P. Wavelength-Scanned Surface-Enhanced Resonance Raman Excitation Spectroscopy. *J. Phys. Chem. C* **2008**, *112*, 19302−19310.
(136) Huang, T.-X.; Huang, S.-C.; Li, M.-H.; Zeng, Z.-C.; Wang, X.; Ren, B. Tip-Enhanced Raman Spectroscopy: Tip-Related Issues. *Anal. Bioanal. Chem.* **2015**, *407*, 8177−8195.
(137) Taguchi, A.; Hayazawa, N.; Furusawa, K.; Ishitobi, H.; Kawata, S. Deep-UV Tip-Enhanced Raman Scattering. *J. Raman Spectrosc.* **2009**, *40*, 1324−1330.
(138) Yang, Z.; Li, Q.; Fang, Y.; Sun, M. Deep Ultraviolet Tip-Enhanced Raman Scattering. *Chem. Commun.* **2011**, *47*, 9131−9133.
(139) Vasconcelos, T. L.; Archanjo, B. S.; Fragneaud, B.; Oliveira, B. S.; Riikonen, J.; Li, C.; Ribeiro, D. S.; Rabelo, C.; Rodrigues, W. N.; Jorio, A.; et al. Tuning Localized Surface Plasmon Resonance in Scanning Near-Field Optical Microscopy Probes. *ACS Nano* **2015**, *9*, 6297−6304.
(140) Johnson, T. W.; Lapin, Z. J.; Beams, R.; Lindquist, N. C.; Rodrigo, S. G.; Novotny, L.; Oh, S.-H. Highly Reproducible Near-Field Optical Imaging with Sub-20-nm Resolution Based on Template-Stripped Gold Pyramids. *ACS Nano* **2012**, *6*, 9168−9174.
(141) Deckert, V.; Deckert-Gaudig, T.; Diegel, M.; Gotz, I.; Langeluddecke, L.; Schneidewind, H.; Sharma, G.; Singh, P.; Singh, P.; Trautmann, S.; et al. Spatial Resolution in Raman Spectroscopy. *Faraday Discuss.* **2015**, *177*, 9−20.
(142) Kim, Z. H.; Leone, S. R. High-Resolution Apertureless Near-Field Optical Imaging Using Gold Nanosphere Probes. *J. Phys. Chem. B* **2006**, *110*, 19804−19809.
(143) You, Y.; Purnawirman, N. A.; Hu, H.; Kasim, J.; Yang, H.; Du, C.; Yu, T.; Shen, Z. Tip-Enhanced Raman Spectroscopy Using Single-Crystalline Ag Nanowire as Tip. *J. Raman Spectrosc.* **2010**, *41*, 1156−1162.
(144) Iwami, M.; Uehara, Y.; Ushioda, S. Preparation of Silver Tips for Scanning Tunneling Microscopy Imaging. *Rev. Sci. Instrum.* **1998**, *69*, 4010−4011.
(145) Dickmann, K.; Demming, F.; Jersch, J. New Etching Procedure for Silver Scanning Tunneling Microscopy Tips. *Rev. Sci. Instrum.* **1996**, *67*, 845−846.
(146) Ren, B.; Picardi, G.; Pettinger, B. Preparation of Gold Tips Suitable for Tip-Enhanced Raman Spectroscopy and Light Emission by Electrochemical Etching. *Rev. Sci. Instrum.* **2004**, *75*, 837−841.
(147) Wang, X.; Liu, Z.; Zhuang, M.-D.; Zhang, H.-M.; Wang, X.; Xie, Z.-X.; Wu, D.-Y.; Ren, B.; Tian, Z.-Q. Tip-Enhanced Raman Spectroscopy for Investigating Adsorbed Species on a Single-Crystal Surface Using Electrochemically Prepared Au Tips. *Appl. Phys. Lett.* **2007**, *91*, 101105.
(148) Jiang, N.; Foley, E. T.; Klingsporn, J. M.; Sonntag, M. D.; Valley, N. A.; Dieringer, J. A.; Seideman, T.; Schatz, G. C.; Hersam, M. C.; Van Duyne, R. P. Observation of Multiple Vibrational Modes in Ultrahigh Vacuum Tip-Enhanced Raman Spectroscopy Combined with Molecular-Resolution Scanning Tunneling Microscopy. *Nano Lett.* **2012**, *12*, 5061−5067.
(149) Li, M.; Lv, R.; Huang, S.; Dai, Y.; Zeng, Z.; Wang, L.; Ren, B. Electrochemical Fabrication of Silver Tips for Tip-Enhanced Raman

DOI: 10.1021/acs.chemrev.6b00343
Chem. Rev. 2017, 117, 4961−4982

Spectroscopy Assisted by a Machine Vision System. *J. Raman Spectrosc.* **2016**, *47*, 808−812.
(150) Kharintsev, S. S.; Hoffmann, G. G.; Fishman, A. I.; Salakhov, M. K. Plasmonic Optical Antenna Design for Performing Tip-Enhanced Raman Spectroscopy and Microscopy. *J. Phys. D: Appl. Phys.* **2013**, *46*, 145501.
(151) Kurouski, D.; Mattei, M.; Van Duyne, R. P. Probing Redox Reactions at the Nanoscale with Electrochemical Tip-Enhanced Raman Spectroscopy. *Nano Lett.* **2015**, *15*, 7956−7962.
(152) Ropers, C.; Neacsu, C. C.; Elsaesser, T.; Albrecht, M.; Raschke, M. B.; Lienau, C. Grating-Coupling of Surface Plasmons onto Metallic Tips: A Nanoconfined Light Source. *Nano Lett.* **2007**, *7*, 2784−2788.
(153) De Angelis, F.; Das, G.; Candeloro, P.; Patrini, M.; Galli, M.; Bek, A.; Lazzarino, M.; Maksymov, I.; Liberale, C.; Andreani, L. C.; et al. Nanoscale Chemical Mapping Using Three-Dimensional Adiabatic Compression of Surface Plasmon Polaritons. *Nat. Nanotechnol.* **2010**, *5*, 67−72.
(154) Yang, L.-K.; Huang, T.-X.; Zeng, Z.-C.; Li, M.-H.; Wang, X.; Yang, F.-Z.; Ren, B. Rational Fabrication of a Gold-Coated AFM TERS Tip by Pulsed Electrodeposition. *Nanoscale* **2015**, *7*, 18225−18231.
(155) Cherukulappurath, S.; Johnson, T. W.; Lindquist, N. C.; Oh, S.-H. Template-Stripped Asymmetric Metallic Pyramids for Tunable Plasmonic Nanofocusing. *Nano Lett.* **2013**, *13*, 5635−5641.
(156) Kalkbrenner, T.; Ramstein, M.; Mlynek, J.; Sandoghdar, V. A Single Gold Particle as a Probe for Apertureless Scanning Near-Field Optical Microscopy. *J. Microsc.* **2001**, *202*, 72−76.
(157) Vakarelski, I. U.; Higashitani, K. Single-Nanoparticle-Terminated Tips for Scanning Probe Microscopy. *Langmuir* **2006**, *22*, 2931−2934.
(158) Kim, W.; Kim, N.; Lee, E.; Kim, D.; Kim, Z. H.; Park, J. W. A Tunable Au Core−Ag Shell Nanoparticle Tip for Tip-Enhanced Spectroscopy. *Analyst* **2016**, *141*, 5066−5070.
(159) Comstock, D. J.; Elam, J. W.; Pellin, M. J.; Hersam, M. C. High Aspect Ratio Nanoneedle Probes with an Integrated Electrode at the Tip Apex. *Rev. Sci. Instrum.* **2012**, *83*, 113704.
(160) Ma, X.; Grüßer, M.; Schuster, R. Plasmonic Nanospheres with a Handle—Local Electrochemical Deposition of Au or Ag at the Apex of Optically Inactive W- or C-Tips. *Appl. Phys. Lett.* **2015**, *106*, 241103.
(161) Nioradze, N.; Chen, R.; Kurapati, N.; Khvataeva-Domanov, A.; Mabic, S.; Amemiya, S. Organic Contamination of Highly Oriented Pyrolytic Graphite as Studied by Scanning Electrochemical Microscopy. *Anal. Chem.* **2015**, *87*, 4836−4843.
(162) Yeo, B.-S.; Stadler, J.; Schmid, T.; Zenobi, R.; Zhang, W. Tip-Enhanced Raman Spectroscopy−Its Status, Challenges and Future Directions. *Chem. Phys. Lett.* **2009**, *472*, 1−13.
(163) Schmid, T.; Yeo, B.-S.; Leong, G.; Stadler, J.; Zenobi, R. Performing Tip-Enhanced Raman Spectroscopy in Liquids. *J. Raman Spectrosc.* **2009**, *40*, 1392−1399.
(164) Zeng, Z.-C.; Huang, S.-C.; Wu, D.-Y.; Meng, L.-Y.; Li, M.-H.; Huang, T.-X.; Zhong, J.-H.; Wang, X.; Yang, Z.-L.; Ren, B. Electrochemical Tip-Enhanced Raman Spectroscopy. *J. Am. Chem. Soc.* **2015**, *137*, 11928−11931.
(165) Li, Z.; Wang, Y.; Kozbial, A.; Shenoy, G.; Zhou, F.; McGinley, R.; Ireland, P.; Morganstein, B.; Kunkel, A.; Surwade, S. P. Effect of Airborne Contaminants on the Wettability of Supported Graphene and Graphite. *Nat. Mater.* **2013**, *12*, 925−931.
(166) Schrader, M. E. Wettability of Clean Metal Surfaces. *J. Colloid Interface Sci.* **1984**, *100*, 372−380.
(167) Weeks, B. L.; Vaughn, M. W.; DeYoreo, J. J. Direct Imaging of Meniscus Formation in Atomic Force Microscopy Using Environmental Scanning Electron Microscopy. *Langmuir* **2005**, *21*, 8096−8098.
(168) Asay, D. B.; Kim, S. H. Effects of Adsorbed Water Layer Structure on Adhesion Force of Silicon Oxide Nanoasperity Contact in Humid Ambient. *J. Chem. Phys.* **2006**, *124*, 174712.
(169) Peica, N.; Röhrig, S.; Rüdiger, A.; Brose, K.; Thomsen, C.; Maultzsch, J. Characterization of Dye Molecules and Carbon Nanostructures by Tip-Enhanced Raman Spectroscopy. *Phys. Status Solidi B* **2009**, *246*, 2708−2712.
(170) Shiotari, A.; Kumagai, T.; Wolf, M. Tip-Enhanced Raman Spectroscopy of Graphene Nanoribbons on Au(111). *J. Phys. Chem. C* **2014**, *118*, 11806−11812.
(171) Chen, C.; Hayazawa, N.; Kawata, S. A 1.7 nm Resolution Chemical Analysis of Carbon Nanotubes by Tip-Enhanced Raman Imaging in the Ambient. *Nat. Commun.* **2014**, *5*, 3312.
(172) Deckert-Gaudig, T.; Kämmer, E.; Deckert, V. Tracking of Nanoscale Structural Variations on a Single Amyloid Fibril with Tip-Enhanced Raman Scattering. *J. Biophotonics* **2012**, *5*, 215−219.
(173) Liao, M.; Jiang, S.; Hu, C.; Zhang, R.; Kuang, Y.; Zhu, J.; Zhang, Y.; Dong, Z. Tip-Enhanced Raman Spectroscopic Imaging of Individual Carbon Nanotubes with Subnanometer Resolution. *Nano Lett.* **2016**, *16*, 4040−4046.
(174) Chiang, N.; Chen, X.; Goubert, G.; Chulhai, D. V.; Chen, X.; Pozzi, E. A.; Jiang, N.; Hersam, M. C.; Seideman, T.; Jensen, L.; et al. Conformational Contrast of Surface-Mediated Molecular Switches Yields Ångstrom-Scale Spatial Resolution in Ultrahigh Vacuum Tip-Enhanced Raman Spectroscopy. *Nano Lett.* **2016**, *16*, 7774−7778.
(175) Roelli, P.; Galland, C.; Piro, N.; Kippenberg, T. J. Molecular Cavity Optomechanics: A Theory of Plasmon-Enhanced Raman Scattering. *Nat. Nanotechnol.* **2016**, *11*, 164−169.
(176) Duan, S.; Tian, G.; Ji, Y.; Shao, J.; Dong, Z.; Luo, Y. Theoretical Modeling of Plasmon-Enhanced Raman Images of a Single Molecule with Subnanometer Resolution. *J. Am. Chem. Soc.* **2015**, *137*, 9515−9518.
(177) Duan, S.; Tian, G.; Luo, Y. Visualization of Vibrational Modes in Real Space by Tip-Enhanced Non-Resonant Raman Spectroscopy. *Angew. Chem.* **2016**, *128*, 1053−1057.
(178) Meng, L.; Yang, Z.; Chen, J.; Sun, M. Effect of Electric Field Gradient on Sub-Nanometer Spatial Resolution of Tip-Enhanced Raman Spectroscopy. *Sci. Rep.* **2015**, *5*, 9240.
(179) Frontiera, R. R.; Shim, S.; Mathies, R. A. Origin of Negative and Dispersive Features in Anti-Stokes and Resonance Femtosecond Stimulated Raman Spectroscopy. *J. Chem. Phys.* **2008**, *129*, 064507.
(180) Zhang, C.; Chen, B. Q.; Li, Z. Y. Optical Origin of Subnanometer Resolution in Tip-Enhanced Raman Mapping. *J. Phys. Chem. C* **2015**, *119*, 11858−11871.
(181) King, F. W.; Van Duyne, R. P.; Schatz, G. C. Theory of Raman Scattering by Molecules Adsorbed on Electrode Surfaces. *J. Chem. Phys.* **1978**, *69*, 4472−4481.
(182) Marinica, D. C.; Kazansky, A. K.; Nordlander, P.; Aizpurua, J.; Borisov, A. G. Quantum Plasmonics: Nonlinear Effects in the Field Enhancement of a Plasmonic Nanoparticle Dimer. *Nano Lett.* **2012**, *12*, 1333−1339.
(183) Zuloaga, J.; Prodan, E.; Nordlander, P. Quantum Description of the Plasmon Resonances of a Nanoparticle Dimer. *Nano Lett.* **2009**, *9*, 887−891.
(184) Latorre, F.; Kupfer, S.; Bocklitz, T.; Kinzel, D.; Trautmann, S.; Grafe, S.; Deckert, V. Spatial Resolution of Tip-Enhanced Raman Spectroscopy - Dft Assessment of the Chemical Effect. *Nanoscale* **2016**, *8*, 10229−10239.
(185) Savage, K. J.; Hawkeye, M. M.; Esteban, R.; Borisov, A. G.; Aizpurua, J.; Baumberg, J. J. Revealing the Quantum Regime in Tunnelling Plasmonics. *Nature* **2012**, *491*, 574−577.
(186) Klingsporn, J. M.; Jiang, N.; Pozzi, E. A.; Sonntag, M. D.; Chulhai, D.; Seideman, T.; Jensen, L.; Hersam, M. C.; Van Duyne, R. P. Intramolecular Insight into Adsorbate−Substrate Interactions Via Low-Temperature, Ultrahigh-Vacuum Tip-Enhanced Raman Spectroscopy. *J. Am. Chem. Soc.* **2014**, *136*, 3881−3887.
(187) Park, K.-D.; Muller, E. A.; Kravtsov, V.; Sass, P. M.; Dreyer, J.; Atkin, J. M.; Raschke, M. B. Variable Temperature Tip-Enhanced Raman Spectroscopy of Single-Molecule Fluctuations and Dynamics. *Nano Lett.* **2016**, *16*, 479−487.
(188) Harvey, C. E.; Weckhuysen, B. M. Surface-and Tip-Enhanced Raman Spectroscopy as Operando Probes for Monitoring and Understanding Heterogeneous Catalysis. *Catal. Lett.* **2015**, *145*, 40−57.

DOI: 10.1021/acs.chemrev.6b00343
Chem. Rev. 2017, 117, 4961−4982

(189) Masango, S. S.; Hackler, R. A.; Henry, A.-I.; McAnally, M. O.; Schatz, G. C.; Stair, P. C.; Van Duyne, R. P. Probing the Chemistry of Alumina Atomic Layer Deposition Using Operando Surface-Enhanced Raman Spectroscopy. *J. Phys. Chem. C* **2016**, *120*, 3822−3833.
(190) Li, X.; Liu, M.; Lee, J.-P.; Ding, D.; Bottomley, L. A.; Park, S.; Liu, M. An Operando Surface Enhanced Raman Spectroscopy (SERS) Study of Carbon Deposition on SOFC Anodes. *Phys. Chem. Chem. Phys.* **2015**, *17*, 21112−21119.
(191) Stadler, J.; Oswald, B.; Schmid, T.; Zenobi, R. Characterizing Unusual Metal Substrates for Gap-Mode Tip-Enhanced Raman Spectroscopy. *J. Raman Spectrosc.* **2013**, *44*, 227−233.
(192) van Schrojenstein Lantman, E. M.; Deckert-Gaudig, T.; Mank, A. J. G.; Deckert, V.; Weckhuysen, B. M. Catalytic Processes Monitored at the Nanoscale with Tip-Enhanced Raman Spectroscopy. *Nat. Nanotechnol.* **2012**, *7*, 583−586.
(193) Huang, Y.-F.; Zhu, H.-P.; Liu, G.-K.; Wu, D.-Y.; Ren, B.; Tian, Z.-Q. When the Signal Is Not from the Original Molecule to Be Detected: Chemical Transformation of Para-Aminothiophenol on Ag During the SERS Measurement. *J. Am. Chem. Soc.* **2010**, *132*, 9244−9246.
(194) Kumar, N.; Stephanidis, B.; Zenobi, R.; Wain, A. J.; Roy, D. Nanoscale Mapping of Catalytic Activity Using Tip-Enhanced Raman Spectroscopy. *Nanoscale* **2015**, *7*, 7133−7137.
(195) Zhang, Z.; Chen, L.; Sun, M.; Ruan, P.; Zheng, H.; Xu, H. Insights into the Nature of Plasmon-Driven Catalytic Reactions Revealed by HV-TERS. *Nanoscale* **2013**, *5*, 3249−3252.
(196) Tallarida, N.; Rios, L.; Apkarian, V. A.; Lee, J. Isomerization of One Molecule Observed through Tip-Enhanced Raman Spectroscopy. *Nano Lett.* **2015**, *15*, 6386−6394.
(197) McNab, I. R.; Polanyi, J. C. Patterned Atomic Reaction at Surfaces. *Chem. Rev.* **2006**, *106*, 4321−4354.
(198) Hla, S.-W.; Bartels, L.; Meyer, G.; Rieder, K.-H. Inducing All Steps of a Chemical Reaction with the Scanning Tunneling Microscope Tip: Towards Single Molecule Engineering. *Phys. Rev. Lett.* **2000**, *85*, 2777−2780.
(199) Altman, E. I.; Baykara, M. Z.; Schwarz, U. D. Noncontact Atomic Force Microscopy: An Emerging Tool for Fundamental Catalysis Research. *Acc. Chem. Res.* **2015**, *48*, 2640−2648.
(200) Schuler, B.; Fatayer, S.; Mohn, F.; Moll, N.; Pavliček, N.; Meyer, G.; Peña, D.; Gross, L. Reversible Bergman Cyclization by Atomic Manipulation. *Nat. Chem.* **2016**, *8*, 220−224.
(201) Zewail, A. H. Femtochemistry: Atomic-Scale Dynamics of the Chemical Bond. *J. Phys. Chem. A* **2000**, *104*, 5660−5694.
(202) Gruenke, N. L.; Cardinal, M. F.; McAnally, M. O.; Frontiera, R. R.; Schatz, G. C.; Van Duyne, R. P. Ultrafast and Nonlinear Surface-Enhanced Raman Spectroscopy. *Chem. Soc. Rev.* **2016**, *45*, 2263−2290.
(203) Link, S.; Burda, C.; Mohamed, M. B.; Nikoobakht, B.; El-Sayed, M. A. Laser Photothermal Melting and Fragmentation of Gold Nanorods: Energy and Laser Pulse-Width Dependence. *J. Phys. Chem. A* **1999**, *103*, 1165−1170.
(204) Fujiwara, H.; Yanagida, S.; Kamat, P. V. Visible Laser Induced Fusion and Fragmentation of Thionicotinamide-Capped Gold Nanoparticles. *J. Phys. Chem. B* **1999**, *103*, 2589−2591.
(205) Littleford, R. E.; Cunningham, D.; Matousek, P.; Towrie, M.; Parker, A. W.; Khan, I.; McComb, D.; Smith, W. E. Surface-Enhanced Resonance Raman Scattering Using Pulsed and Continuous-Wave Laser Excitation. *J. Raman Spectrosc.* **2005**, *36*, 600−605.
(206) Frontiera, R. R.; Henry, A.-I.; Gruenke, N. L.; Van Duyne, R. P. Surface-Enhanced Femtosecond Stimulated Raman Spectroscopy. *J. Phys. Chem. Lett.* **2011**, *2*, 1199−1203.
(207) Klingsporn, J. M.; Sonntag, M. D.; Seideman, T.; Van Duyne, R. P. Tip-Enhanced Raman Spectroscopy with Picosecond Pulses. *J. Phys. Chem. Lett.* **2014**, *5*, 106−110.
(208) Pozzi, E. A.; Sonntag, M. D.; Jiang, N.; Chiang, N.; Seideman, T.; Hersam, M. C.; Van Duyne, R. P. Ultrahigh Vacuum Tip-Enhanced Raman Spectroscopy with Picosecond Excitation. *J. Phys. Chem. Lett.* **2014**, *5*, 2657−2661.
(209) Wickramasinghe, H. K.; Chaigneau, M.; Yasukuni, R.; Picardi, G.; Ossikovski, R. Billion-Fold Increase in Tip-Enhanced Raman Signal. *ACS Nano* **2014**, *8*, 3421−3426.
(210) Ichimura, T.; Hayazawa, N.; Hashimoto, M.; Inouye, Y.; Kawata, S. Application of Tip-Enhanced Microscopy for Nonlinear Raman Spectroscopy. *Appl. Phys. Lett.* **2004**, *84*, 1768−1770.
(211) Ichimura, T.; Hayazawa, N.; Hashimoto, M.; Inouye, Y.; Kawata, S. Tip-Enhanced Coherent Anti-Stokes Raman Scattering for Vibrational Nanoimaging. *Phys. Rev. Lett.* **2004**, *92*, 220801.
(212) Hayazawa, N.; Ichimura, T.; Hashimoto, M.; Inouye, Y.; Kawata, S. Amplification of Coherent Anti-Stokes Raman Scattering by a Metallic Nanostructure for a High Resolution Vibration Microscopy. *J. Appl. Phys.* **2004**, *95*, 2676−2681.
(213) Furusawa, K.; Hayazawa, N.; Catalan, F. C.; Okamoto, T.; Kawata, S. Tip-Enhanced Broadband CARS Spectroscopy and Imaging Using a Photonic Crystal Fiber Based Broadband Light Source. *J. Raman Spectrosc.* **2012**, *43*, 656−661.
(214) Opilik, L.; Dogan, Ü.; Li, C.-Y.; Stephanidis, B.; Li, J.-F.; Zenobi, R. Chemical Production of Thin Protective Coatings on Optical Nanotips for Tip-Enhanced Raman Spectroscopy. *J. Phys. Chem. C* **2016**, *120*, 20828−20832.

DOI: 10.1021/acs.chemrev.6b00343
Chem. Rev. 2017, 117, 4961−4982